ANALYSIS OF NONLINEAR EFFECTS AND THEIR MITIGATION IN FIBER-OPTIC COMMUNICATION SYSTEMS

ANALYSIS OF NONLINEAR EFFECTS AND THEIR MITIGATION IN FIBER-OPTIC COMMUNICATION SYSTEMS

BY

MAHDI MALEKIHA, B.Sc.

A THESIS

SUBMITTED TO THE DEPARTMENT OF ELECTRICAL & COMPUTER ENGINEERING

AND THE SCHOOL OF GRADUATE STUDIES

OF MCMASTER UNIVERSITY

IN PARTIAL FULFILMENT OF THE REQUIREMENTS

FOR THE DEGREE OF

MASTER OF APPLIED SCIENCE

Master of Applied Science (2011) McMaster University

(Electrical & Computer Engineering) Hamilton, Ontario, Canada

TITLE:	ANALYSIS OF NONLINEAR EFFECTS AND THEIR MITIGATION IN FIBER-OPTIC COMMUNICATION SYSTEMS
AUTHOR:	MAHDI MALEKIHA B.Sc., (Electrical Engineering) Isfahan University of Technology, Isfahan, Iran
SUPERVISOR:	Dr. Shiva Kumar
NUMBER OF PAGES:	xiv, 96

To my beloved family, for your continued support and encouragment

Abstract

The rapid development of fiber optic communication systems requires higher transmission data rate and longer reach. This thesis deals with the limiting factors in design of long-haul fiber optic communication systems and the techniques used to suppress their resulting impairments. These impairments include fiber chromatic dispersion, the Ker nonlinearity and nonlinear phase noise due to amplified spontaneous emission.

In the first part of this thesis, we investigate the effect of amplified spontaneous noise in quasi-linear systems. In quasi-linear systems, inline optical amplifiers change the amplitude of the optical field envelope randomly and fiber nonlinear effects such as self phase modulation (SPM) convert the amplitude fluctuations to phase fluctuations which is known as nonlinear phase noise. For M-ary phase shift keying (PSK) signals, symbol error probability is determined solely by the probability density function (PDF) of the phase. Under the Gaussian PDF assumption, the phase variance can be related to the symbol error probability for PSK signals. We implemented the simulation based on analytical phase noise variance and Monte-Carlo simulation, and it is found that the analytical approximation is in good agreement with numerical simulations. We have developed analytical expressions for the linear and nonlinear phase noise variance due to SPM using second-order perturbation theory. It is found

that as the transmission reach and/or lunch power increase, the variance of the phase noise calculated using first order perturbation theory becomes inaccurate. However, the variance calculated using second order perturbation theory is in good agreement with numerical simulations. We have also showed that the analytical formula given in this chapter for the variance of nonlinear phase noise can be used as a design tool to investigate the optimum system design parameters such as average power and dispersion maps for coherent fiber optic systems based on phase shift keying due to the fact that the numerical simulation of nonlinear Schrodinger (NLS) equation is time consuming, however, the analytical method based on solving NLS equation using perturbation approximation is quite efficient and therefore the analytical variance can be obtained more easily without requiring extensive computational efforts, and also with fairly good accuracy.

In the second part of this thesis, an improved optical signal processing using highly nonlinear fibers is studied. This technique, optical backward propagation (OBP), can compensate for the fiber dispersion and nonlinearity using optical nonlinearity compensators (NLC) and dispersion compensating fibers (DCF), respectively. In contrast, digital backward propagation (DBP) uses the high-speed digital signal processing (DSP) unit to compensate for the fiber nonlinearity and dispersion digital domain. NLC imparts a phase shift that is equal in magnitude to the nonlinear phase shift due to Fiber propagation, but opposite in sign. In principle, BP schemes could undo the deterministic (bit-pattern dependent) nonlinear impairments, but it can not compensate for the stochastic nonlinear impairments such as nonlinear phase noise. We also introduced a novel inline optical nonlinearity compensation (IONC) technique. Our Numerical simulations show that the transmission performance can be greatly

improved using OBP and IONC. Using IONC, the transmission reach becomes almost twice of DBP. The advantage of OBP and IONC over DBP are as follows: OBP/IONC can compensate the nonlinear impairments for all the channels of a wavelength division multiplexed system (WDM) in real time while it would be very challenging to implement DBP for such systems due to its computational cost and bandwidth requirement. OBP and IONC can be used for direct detection systems as well as for coherent detection while they provide the compensation of dispersion and nonlinearity in real time, but DBP works only for coherent detection and currently limited to off-line signal processing.

Acknowledgements

I would like to express my most sincere gratitude to my supervisor, Dr. Shiva Kumar. It is an honor for me to study under his supervision. I appreciate all his contributions of time, ideas, and funding to make my M.Sc. experience productive and stimulating. The joy and enthusiasm he has for his research was contagious and motivational for m, even during tough times in the M.Sc. pursuit.

I also would like to appreciate all colleagues of Photonic CAD Laboratory. They have been a source of friendships as well as good advice and collaboration.

For this dissertation, I would like to thank my defense committee members: Dr. Mohamed Bakr and Dr. Chih-Hung Chen for their time, interest, helpful comments and insightful questions.

My time at McMaster was made enjoyable in large part due to the many friends and groups that became a part of my life. I am grateful for time spent with roommates and friends, and for many other people and memories.

Lastly, I would like to thank my family for all their love and encouragement. For my parents who raised me with a love of science and supported me in all my pursuits. And most of all for my loving, supportive, encouraging, and patient wife Mehrnoosh whose faithful support during the final stages of this M.Sc. is so appreciated.

Notation and abbreviations

ASE Amplified Spontaneous Emission

BER Bit Error Rate

CD Chromatic Dispersion

DGD Differential Group Delay

DCF Dispersion-Compensating Fiber

DPSK Differential Phase-Shift Keying

PSK Phase-Shift Keying

QAM Quadrature Amplitude Modulation

FNL Fiber Nonlinearity

FFT Fast Fourier Transform

FWM Four-Wave Mixing

IFWM Intra-channel Four-Wave Mixing

XPM Cross-Phase Modulation

IXPM Intra-channel Cross-Phase Modulation

IONC Inline optical nonlinearity compensation

NLSE Nonlinear Schrodinger Equation

NPS Nonlinear Phase Shift **PMD** Polarization Mode Dispersion

PSP Principle State of Polarization

PDE Partial Differential Equation

SPM Self-Phase Modulation

SMF Single Mode Fiber

SNR Signal-Noise Ratio

SSFS Split-Step Fourier Transform

DFS Dispersion-Shifted Fiber

WDM Wavelength-Division Multiplexing

EDFA Erbium-Doped Fiber Amplifier

OE Optical-to-Electrical

EO Electrical-to-Optical

GVD Group velocity Dispersion

ISI Inter-Symbol Interference

FP Forward propagation

DBP Digital Backward Propagation

OBP Optical Backward Propagation

NRZ Non-Return-to-Zero

NLC Nonlinearity Compensator

PRBS Pseudo-Random Bit Sequence

FEC Forward Error Correction

HNLF Highly Nonlinear Fiber

Contents

List of Figures

Chapter 1

Introduction

A communication system transmits information from one place to another, whether separated by a few kilometers or by transoceanic distances. Information is often carried by an electromagnetic carrier wave whose frequency can vary from a few megahertz to several hundred terahertz. In the virtually infinite broad electromagnetic spectrum, there are only two windows that have been largely used for modern-day broadband communications. The first window spans from the long-wave radio to millimeter wave, or from 100 KHz to 300 GHz in frequency, whereas the second window lies in the infrared lightwave region, or from 30 THz to 300 THz in frequency. The first window provides the applications that we use in our daily lives, including broadcast radio and TV, wireless local area networks (LANs), and mobile phones. These applications offer the first meter or first mile access of the information networks to the end user with broadband connectivity or the mobility in the case of the wireless systems. Nevertheless, most of the data rates are capped below gigabit per second (Gb/s) primarily due to the lack of the available spectrum in the RF microwave range. In contrast, due to the enormous bandwidth over several terahertz

(THz) in the second window, the lightwave systems can provide a staggering capacity of 100 Tb/s and beyond. In fact, the optical communication systems, or fiber-optic systems in particular, have become indispensable as the backbone of the modern-day information infrastructure. While initial deployment of optical fiber was mainly for long-haul or submarine transmission, lightwave systems are currently in almost all metro networks. Fiber-to-the-premise (FTTP) and fiber-to-the-home (FTTH) are being considered seriously in most parts of the world right now [1].

Optical communication systems have been deployed worldwide since 1980 and have indeed revolutionized the technology behind telecommunications. Indeed, the lightwave technology, together with microelectronics, is believed to be a major factor in the advent of the information age.

1.1 Evolution of Fiber-Optic Communications

A point-to-point fiber-optic communication system, the simplest kind of lightwave system, consists of a transmitter, followed by transmission channel (fiber), and then a receiver. The evolution of fiber-optic communications has been promoted along with the advent of the above three major components in a fiber communication system. In 1960, the invention and the realization of laser [2] provided a coherent source for transmitting information using lightwaves. After that, In 1966, Kao and Hockman proposed the idea of using the optical fiber as the lightwave transmission medium despite the fact that optical fiber at the time suffered unacceptable loss (over 1000 dB/Km). They argued that the attenuation in fibers available at the time was caused by impurities, which could be removed. Their prophetic prediction of 20 dB/Km for telecom-grade optical fiber was realized 5 years later by researchers from Corning

[3]. In 1979, the low loss fiber was realized at the operating wavelength of 1550 nm [4] with a loss of 0.2 dB/Km. The simultaneous availability of stable optical source (laser) and a low-loss optical fiber led to an extensive research efforts and rapid development of fiber-optic communication systems, which can be grouped into five distinct generations [5]. A commonly used figure of merit for point-to-point communication systems is the bit rate-distance product, BL, where B is the bit rate and L is the repeater spacing. In every generation, BL increases initially but then begins to saturate as the technology matures. Each new generation brings a fundamental change that helps to improve the system performance further.

The first-generation of lightwave systems operated near 800 nm and used GaAs semiconductor lasers. They operated at a bit rate of 45 Mb/s and allowed repeater spacings of up to 10 Km. The repeater spacing of the first-generation lightwave systems was limited by fiber dispersion which lead to pulse-spreading at the operating wavelength of 800 nm. In 1970s that the repeater spacing increased considerably by operating the lightwave system in the wavelength region near 1300 nm, where optical fibers exhibit minimum dispersion Furthermore, fiber loss is below 1 dB/Km. This realization led to a worldwide effort for the development of InGaAsP semiconductor lasers and detectors operating near 1300 nm. The second generation of fiber-optic communication systems became available in the early 1980s, but the bit rate of early systems was limited to below 100 Mb/s because of intermodal dispersion in multimode fibers. This limitation was overcome by the use of single-mode fibers. By 1987, second-generation lightwave systems, operating at bit rates of up to 1.7 Gb/s with a repeater spacing of about 50 Km, were commercially available.

The repeater spacing of the second-generation lightwave systems was limited by

the fiber losses at the operating wavelength of 1300 nm (typically 0.5 dB/km). Losses of silica fibers become minimum near 1550 nm. Indeed, a 0.2 dB/Km loss was realized in 1979 in this spectral region. The drawbacks of 1550 nm systems were a large fiber dispersion near 1550 nm, and the conventional InGaAsP semiconductor lasers could not be used because of pulse spreading occurring as a result of simultaneous oscillation of several longitudinal modes. The dispersion problem can be overcome either by using dispersion-shifted fibers designed to have minimum dispersion near 1550 nm or by limiting the laser spectrum to a single longitudinal mode. For a dispersion shifted fiber (DSF) [6] the zero chromatic dispersion (CD) is shifted to minimum-loss window at 1550 nm from 1300 nm by controlling the waveguide dispersion and dopant-dependent material dispersion such that transmission fiber with both low dispersion and low attenuation can be achieved. Third-generation lightwave systems operating at 2.5 Gb/s became available commercially in 1990. Such systems are capable of operating at a bit rate of up to 10 Gb/s. The best performance is achieved using dispersion-shifted fibers in combination with lasers oscillating in a single longitudinal mode.

A drawback of third-generation 1550 nm systems is that the signal is regenerated periodically by using optoelectronic repeaters, spaced apart typically by 60 - 70 Km, in which the optical signal is first convert to the electrical current and then regenerate by modulating an optical source. The repeater spacing can be increased by making use of a homodyne or heterodyne detection schemes because its use improves receiver sensitivity. These optoelectronic regenerating procedures are not suitable for multi-channel lightwave systems because each single wavelength needs a separate optoelectronic repeater, which leads to high cost and excessive system complexity.

Another drawback of using electronic repeaters is that due to high data rate in optical communication systems, the high speed electronic devises are required which is very hard and expensive to make. The advent of optical amplifiers, which amplify the optical bit stream directly without requiring conversion of the signal to the electric domain, revolutionized the development of fiber optic communication systems in the late 1980s. Only adding noise to the signal, optical amplifiers are especially valuable for wavelength division multiplexed (WDM) lightwave systems as they can amplify many channels simultaneously without crosstalk and distortion.

The fourth generation of lightwave systems makes use of optical amplification for increasing the repeater spacing and of wavelength division multiplexing for increasing the bit rate. The optical amplification was first realized using semiconductor laser amplifiers in 1983, then Raman amplifiers in 1986 [7], and later using optically pumped rare earth erbium doped fiber amplifier (EDFA) in 1987 [8]. The low-noise, high-gain and wide-band amplification characteristics of EDFAs stimulated the development of transmitting signal using multiple carriers simultaneously, which can be implemented using a wavelength division multiplexing scheme. WDM is basically the same as the frequency-division multiplexing (FDM) as the wavelength and frequency are related $\lambda = v/f$ where v is the speed of light and f is the frequency. In optical WDM system, multiplexing and demultiplexing are realized at transmitter and receiver respectively using arrow waveguide grating (AWG). The advent of the WDM technique started a revolution in optical communication networks due to the fact that the capacity of the system can be increased simply by increasing the number of channels without deploying more fibers. That resulted in doubling of the system capacity every 6 months or so, and led to lightwave systems operating at a bit rate of 10 Tb/s by

2001. Commercial terrestrial systems with the capacity of 1.6 Tb/s were available by the end of 2000, and the plans were underway to extend the capacity toward 6.4 Tb/s. Given that the first-generation systems had a capacity of 45 Mb/s in 1980, it is remarkable that the capacity has jumped by a factor of more than 10,000 over a period of 20 years.

The fifth generation of fiber-optic communication systems is concerned with extending the wavelength range over which a WDM system can operate simultaneously. While WDM systems can greatly improve the capacity of fiber optic transmission systems by increasing the number of channels, achievable data rate is limited by the bandwidth of optical amplifiers and ultimately by the fiber itself. The conventional wavelength window, known as the C-band, covers the wavelength range 1530 - 1570 nm. It is being extended on both the long- and short-wavelength sides, resulting in the L- and S-bands, respectively. The Raman amplification technique can be used for signals in all three wavelength bands. Moreover, a new kind of fiber, known as the dry fiber has been developed with the property that fiber losses are small over the entire wavelength region extending from 1300 to 1650 nm. Availability of such fibers and new amplification schemes may lead to lightwave systems with thousands of WDM channels.

The fifth-generation systems also attempt to increase the data rate of each channel within the WDM signal. This could be addressed by improving the signal spectral efficiency. The signal spectral efficiency is measure in bit/s/Hz, and can be increased using various spectrally efficient modulation schemes, such as M-ary phase shift keying (MPSK) and quadrature amplitude modulation (QAM) and/or polarization division multiplexing (PDM) technique. In fiber-optical transmission systems the transmitted

signal power can not be arbitrary large due to the fiber nonlinearity and therefore it requires a high-sensitivity optical receiver for a noise-limited transmission system. The power efficiency can be improved by minimizing the required average signal power or optical signal to noise ratio (OSNR) at a, given level of bit error rate (BER). In a conventional fiber optic communication system, the intensity of the optical carrier is modulated by the electrical information signal and at the receiver, the optical signal, transmitted through fiber link,is directly detected by a photo-diode acting as a square-law detector, and converted into the electrical domain. This simple deployment of intensity modulation (IM) on the transmitter side and direct detection (DD) at the receiver end called intensity modulation-direct detection (IM-DD) scheme. Apparently, due to the power law of a photo diode, the phase information of the transmitted signal is lost when direct detection is used, which prevents the use of phase-modulated modulation schemes, like MPSK and QAM. Therefore, both spectral efficiency and power efficiency are limited in a fiber-optic system using direct detection.

In contrast, like many wireline and wireless telecommunication systems, homodyne or heterodyne detection schemes can be introduced to fiber optic communications. This kind of system are referred to as coherent fiber optic systems. The coherent optical communication systems have been extensively studied during 1980s due to high receiver sensitivity. However, coherent communication systems were not commercialized because of the practical issues associated with phase locked loops (PLLs) to align the phase of local oscillator with the output of the fiber optic link and with the emergence of the EDFA, the former advantage of a higher receiver sensitivity compared to direct detection disappeared, the more so as the components were complex and costly.

Nowadays however, coherent optical systems are reappearing as an area of interest. The linewidth requirements have relaxed and sub-megahertz linewidth lasers have recently been developed. More recently, the high-speed digital signal processing available allows for the implementation of critical operations like phase locking, frequency synchronization and polarization control in the electronic domain through digital means. Former concepts for carrier synchronization with optical phase locked loops (OPLL) can be replaced by subcarrier OPLLs or digital phase estimation. Thus, under the new circumstances, the chances of cost effectively manufacturing stable coherent receivers are increasing.

In addition to the already mentioned potentials of spectral efficiency, coherent detection provides several advantages. Coherent detection is very beneficial within the design of optical high-order modulation systems, because all the optical field parameters (amplitude, phase frequency and polarization) are available in the electrical domain. Therefore, the demodulation schemes are not limited to the detection of phase differences as for direct detection, but arbitrary modulation formats and modulation constellations can be received. Furthermore, the preservation of the temporal phase enables more effective methods for the adaptive electronic compensation of transmission impairments like chromatic dispersion and nonlinearities. When used in WDM systems, coherent receivers can offer tunability and enable very small channel spacings, since channel separation can be performed by high-selective electrical filtering.

1.2 Thesis Contribution

This thesis deals with analysis of nonlinear phase noise and a novel optical nonlinearity compensation technique to mitigate fiber impairments in coherent fiber optic communication systems, and it is organized as follows. In chapter 2, a literature on the major fiber optic communication systems impairments such as the fiber Ker effect and chromatic dispersion is reviewed and coherent transmission technology, dispersion compensation techniques and backward propagation (BP) are discussed.

In chapter 3, we investigate the effect of amplified spontaneous noise in quasi-linear systems. In quasi-linear systems, dispersive effects are much stronger than the nonlinear effects, and therefore, the fiber nonlinearity can be considered as a small perturbation on the linear system. We have developed analytical expressions for the linear and nonlinear phase noise variance due to noise added by amplifiers and SPM interaction using second-order perturbation theory. For M-ary phase shift keying (PSK) signals, symbol error probability is determined solely by the probability density function (PDF) of the phase. Under the Gaussian PDF assumption, the phase variance can be related to the symbol error probability for PSK signals. We implemented the simulation based on analytical phase noise variance and Monte-Carlo simulation, and it is found that the analytical approximation is in good agreement with numerical simulations.

In chapter 4, an improved optical signal processing using highly nonlinear fibers is studied. This technique, optical backward propagation (OBP), can compensate for the fiber nonlinearity using optical nonlinearity compensators (NLC) and dispersion using dispersion compensating fibers (DCF). NLC imparts a phase shift that is

equal in magnitude to the nonlinear phase shift due to fiber propagation, but opposite in sign. In principle, BP schemes could undo the deterministic (bit-pattern dependent) nonlinear impairments, but it can not compensate for the stochastic nonlinear impairments such as nonlinear phase noise. We also introduced a novel inline optical nonlinearity compensation (IONC) technique which incorporate inline optical nonlinear compensators and dispersion compensating fiber at receiver. We have implemented OBP and IONC techniques numerically and compared their performance with convectional digital backward propagation (DBP) for multi-level quadrature amplitude modulation (QAM) signals. The transmission reach without OBP, DBP and inline nonlinearity compensation (but with DCF) is limited to 240 Km at the forward error correction (FEC) limit. The maximum reach can be increased to 1040 Km and 1440 Km using OBP and IONC, respectively and in the case of DBP maximum reach is 800 Km. We also investigated the effect using imperfect optical nonlinearity compensators in OBP and IONC, and we found that these techniques have reasonably good tolerance and there is no performance degrading in this situation.

In chapter 5, the conclusions of present works and future plans are given. All references are placed at the end of this thesis.

This research work has resulted following publication and manuscript:

M. Malekiha and S. Kumar, "Second-Order theory for Nonlinear Phase Noise in Coherent Fiber-Optic Systems Based on Phase Shift Keying", CCECE, P. 466-469, 2011.

Chapter 2

Literature Background

2.1 Fiber Optic Communication Systems Impairments

In fiber optic communication systems, linear impairments are due to the fiber loss, chromatic dispersion (CD) and polarization mode dispersion (PMD). Optical power loss dues to light propagation inside the fiber results from absorption and scattering and it can be easily compensated by optical amplifiers. CD and PMD are the main linear impairments for optical communication systems. Major degrading effects due to fiber nonlinearity are self phase modulation (SPM), cross phase modulation (XPM), four wave mixing (FWM), stimulated Raman Scattering (SRS) and Stimulated Brillioun Scattering (SBS).

In its simplest form, an optical fiber consists of a central glass core surrounded by a cladding layer whose refractive index n_c is slightly lower than the core index n_l. For an understanding of evolution of optical field in the optical fiber, it is necessary

to consider the theory of electromagnetic wave propagation in dispersive nonlinear media. Like all electromagnetic phenomena, the propagation of optical fields in fibers is governed by Maxwells equations. For standard single mode fibers (SMFs), the pulse,propagation is described by nonlinear Schrodinger equation (NLSE). it describes the evolution of optical field at the transmission distance z as [9]

$$\frac{\partial A}{\partial z} - \beta_1 \frac{\partial A}{\partial t} + \frac{i\beta_2}{2}\frac{\partial^2 A}{\partial t^2} - \frac{\beta_3}{6}\frac{\partial^3 A}{\partial t^3} + \frac{\alpha}{2}A = i\gamma\left[|A^2|A + \frac{i}{\omega_0}\frac{\partial |A^2|A}{\partial t} - T_R A\frac{\partial |A|^2}{\partial t}\right] \quad (2.1)$$

where A represents the optical field envelope, γ is the nonlinearity coefficient, α is the attenuation constant, β_1, β_2 and β_3 are first-order, second- and third-order derivations of the propagation constant β about the center frequency ω_0 and they are related to the dispersion of the optical fiber, and T_R can be related to the slope of the Raman gain spectrum and is usually estimated to be 3 fs at wavelengths near 1.5 μm. The term proportional to β_3 account for third-order dispersion, and only becomes important for ultrashort pulses, because of their wide bandwidth. The last two terms in the right side of the equation are related to the effects of self-steeping and stimulated Raman scattering, respectively. For pulses of width $To > 5$ ps, the parameters $1/(\omega_0 T_0)$ and T_R/T_0 become so small (< 0.001) that the last two terms in Eq. (2.1) can be neglected on such condition, and if the reference time frame moves with pulse at the group velocity, v_g i.e. $T = t - z/v_g = t - \beta_1 z$, the Eq. (2.1) can be simplified

$$\frac{\partial A}{\partial z} + \frac{i\beta_2}{2}\frac{\partial^2 A}{\partial t^2} + \frac{\alpha}{2}A = i\gamma|A^2|A \quad (2.2)$$

2.1.1 Chromatic Dispersion

Chromatic dispersion, or group velocity dispersion (GVD), is primarily the cause of performance limitation in the long haul 10 Gb/s and beyond fiber optic communication systems. Dispersion is the spreading out of a light pulse in time as it propagates down the fiber. As a result short pulses become longer, which leads to significant inter symbol interference (lSI), and therefore, severely degrades the performance. Single mode fibers (SMFs), effectively eliminate inter-modal dispersion by limiting the number of modes to just one through a much smaller core diameter. However, the pulse broadening still occurs in SMFs due to intra-modal dispersion which is described as follows.

When an electromagnetic wave interacts with the bound electrons of a dielectric, the medium response, in general, depends on the optical frequency ω. This property manifests through the frequency dependence of the refractive index $n(\omega)$. Because the velocity of light is determined by $c/n(\omega)$, the different frequency components of the optical pulse would travel at different speeds. This phenomenon is called group velocity dispersion or chromatic dispersion to emphasize its frequency dependent nature.

Assuming the spectral width of the pulse to be $\Delta\omega$, at the output of the optical fiber, the pulse broadening can be estimated as [5]

$$\Delta T \sim L\frac{d^2\beta}{d\omega^2}\Delta\omega = L\beta_2\Delta\omega \tag{2.3}$$

where $\beta_2 = d^2\beta/d\omega^2$ is known as GVD parameter and L is the fiber length. It can be seen from Eq,(2.3), that the amount of pulse broadening is determined by the spectral

width of pulse, $\Delta\omega$.

The dispersion induced spectrum broadening would be very important even without nonlinearity for high data-rate transmission systems (> 2.5 Gb/s), and it could limit the maximum error-free transmission distance. The effects of dispersion can be described by expanding the mode propagation constant, β, at any frequency ω in terms of the propagation constant and its derivatives at some reference frequency ω_0 using the Taylor series,

$$\beta(\omega) = \beta_0 + \beta_1(\omega - \omega_0) + \frac{1}{2}\beta_2(\omega - \omega_0)^2 + ... \tag{2.4}$$

where

$$\beta_m(\omega) = \left[\frac{d^m\beta}{d\omega^m}\right]_{\omega=\omega_0} \quad (m = 0, 1, 2, ...) \tag{2.5}$$

It is easy to get first-order and second-order derivatives from Eqs. (2.4) and (2.5)

$$\beta_1 = \frac{1}{c}\left[n + \omega\frac{dn}{d\omega}\right] = \frac{1}{v_g} \tag{2.6}$$

and

$$\beta_2 = \frac{1}{c}\left[2\frac{dn}{d\omega} + \omega\frac{d^2n}{d\omega_2}\right] \sim \frac{\lambda^3}{2\pi c^2}\frac{d^2n}{d\lambda^2} \tag{2.7}$$

where c is the speed of light vacuum and λ is the wavelength. β_1 is the inverse group velocity, and β_2 is the second order dispersion coefficient. If the signal bandwidth is much smaller than the carrier frequency ω_0, we can truncate the Taylor series after the second term on the right hand side. As the spectral width of the signal transmitted over the fiber increases, it may be necessary to include the higher order dispersion coefficients such as β_3 and β_4. The wavelength where $\beta_2 = 0$ is called zero dispersion

wavelength λ_D. However, there is still dispersion at wavelength λ_D due to higher order dispersion and they should be considered in this case. This feature can be understood by noting that $\beta_2 = 0$ can not be made zero at all wavelengths contained within the pulse spectrum centered at λ_D.

Dispersion parameter, D, is another parameter related to the difference in arrival time of pulse spectrum which more often being used. With a dispersion coefficient of D, two signals with wavelength separation of $\Delta\lambda$ walk-off by a time of $D\Delta\lambda L$ after a distance of L. The relationship between D, β_1 and β_2 can be found as following

$$D = \frac{d\beta_1}{d\lambda} = -\frac{2\pi c}{\lambda^2}\beta_2 \approx -\frac{\lambda}{c}\frac{d^2 n}{d\lambda^2} \tag{2.8}$$

From Eq. (2.8) it can be understood that D has the opposite sign with β_2. If $\lambda < \lambda_D$, $\beta_2 < 0$ (or $D > 0$), It is said that optical signal exhibit normal dispersion. In the normal dispersion regime high-frequency components of optical signal travel slower than low-frequency components. On the contrary, When $\lambda > \lambda_D$, $\beta_2 > 0$ (or $D > 0$), it is said to exhibit anomalous dispersion. In the anomalous dispersion regime high-frequency components of optical signal travel faster than low-frequency components. The anomalous dispersion regime is of considerable interest for the study of nonlinear effects, because it is in this regime that optical fibers support solitons through a balance between the dispersive and nonlinear effects.

The impact of the group velocity dispersion can be conventionally described using the dispersion length define as [9]

$$L_D = \frac{T_0^2}{\beta_2} \tag{2.9}$$

where T_0 is the temporal pulse width. This length provides a scale over which the dispersive effect becomes significant for pulse evolution along a fiber. Dispersion and specially GVD plays an important role in signal transmission over fibers. The interaction between dispersion and nonlinearity is an important issue in lightwave system design.

2.1.2 Fiber Kerr Nonlinearities

The response of any dielectric to light becomes nonlinear for intense electromagnetic fields, and optical fibers are no exception. The optical fiber medium can only be approximated as a linear medium when the lunch power is sufficiently low. For the long-haul fiber optic transmission system and wideband wavelength division multiplexed (WDM) systems, to combat accumulated noise added by the amplifier chain along the transmission fiber link, the launch power must be increased to keep signal to noise ratio (SNR) high enough for the error-free detection at receiver. As the launch power increases, the nonlinearity of fiber becomes significant and leading to severe performance degrading. Nonlinear effects in optical fibers are mainly due to two causes. One root cause lies in the fact that the index of refraction of many materials, including glass, is a function of light intensity. The origin of this nonlinear response is related to anharmonic motion of bound electrons under the influence of an applied field. This phenomenon is called the Kerr effect and it is discovered in 1875 by John Kerr. The second root cause is the nonelastic scattering of photons in fibers, which results in stimulated Raman and stimulated Brillouin scattering phenomena. These are in addition to the dependence of the index of refraction on wavelength,

which gives rise to dispersion effects. The refractive index can be written as

$$n(\omega, P) = n_0(\omega) + n_2 \frac{P}{A_{eff}} \tag{2.10}$$

where n_0 is the linear part of the refractive index, n_2 is the Kerr coefficient with typical value of $2.2 - 3.4 \times 10^{-20}$ m^2/W, P is the optical power, and A_{eff} is the effective core area. In fiber optics, the Kerr coefficient is small compared to most other nonlinear media by at least two orders of magnitude. In spite of the intrinsically small values of the nonlinear coefficients in fused silica, the nonlinear effects in optical fibers can be observed at relatively low power levels. This is possible because of two important characteristics of single mode fiber (SMF): (i) a small effective core area and (ii) extremely low loss (< 1 dB/Km). The dependence of the refractive index on the light intensity results in the propagation constant, β, varying as the light intensity due to $\beta = 2\pi n/\lambda$, and the propagation constant can be written as

$$\beta(\omega, P) = \beta_0(\omega) + \frac{2\pi n_2}{\lambda A_{eff}} P \tag{2.11}$$

where $\beta_0(\omega)$ is the propagation constant in the absence of nonlinear effects, and

$$\gamma = \frac{2\pi n_2}{\lambda A_{eff}} \tag{2.12}$$

is known as the fiber nonlinear coefficient. The total nonlinear phase shift due to the Kerr effect after the distance L is given by

$$\phi_{NL} = \int_0^L [\beta - \beta_0] dz \tag{2.13}$$

Substituting Eq. (2.11) in Eq. (2.12), using Eq. (2.13) and noticing that

$$P(z) = P_0 \exp(-\alpha z) \tag{2.14}$$

where P_0 is the launch power, and α is the loss coefficient, we obtain [10]

$$\phi_{NL} = \gamma P_0 \int_0^L \exp(-\alpha z) dz = \gamma P_0 \frac{1 - \exp(-\alpha L)}{\alpha} = \frac{L_{eff}}{L_{NL}} \tag{2.15}$$

where

$$L_{eff} = \frac{1 - \exp(-\alpha L)}{\alpha} \tag{2.16}$$

is the effective length, and

$$L_{NL} = \frac{1}{\gamma P_0} \tag{2.17}$$

is the nonlinear length. Physically, the nonlinear length, L_{NL}, indicates the distance at which the nonlinear phase shift reaches 1 radian, and it provides a length scale over which the nonlinear effects become relevant for optical fibers. It can be seen from Eq. (2.15) that the fiber nonlinear effect enhances when L_{NL} decreases, or equivalently power P_0 increases. There are three types of fiber nonlinearities due to the Kerr effect. Type (i) self phase modulation (SPM) (ii) cross phase modulation (XPM), and (iii) four wave mixing (FWM). The SPM, Refers to the self-induced power-dependent phase shift experienced by an optical field during its propagation in the optical fiber as shown in Eq. (2.15), and it is responsible for spectral broadening of the optical pulses. Interacting with fiber dispersion, the SPM can cause temporal pulse broadening (in normal dispersion regime ($\beta_2 > 0$)), or pulse compression (in anomalous dispersion regime ($\beta_2 < 0$). The well known interaction of SPM with

anomalous dispersion is the formation of solitons. The cross phase modulation causes the nonlinear phase shift due to optical pulses from other channels or from other state of polarization. The XPM effects are quite important for WDM lightwave systems since the phase of each optical channel is affected by both the average power and the bit pattern of all other channels.

In WDM systems, the nonlinear phase shift in $K-th$ channel can be written as

$$\phi_{NL} = \gamma L_{eff} P_0^{(k)} + 2 \sum_{h=1, h\neq k}^{N} \gamma L_{eff} P_0^{(h)} \tag{2.18}$$

where $P_0^{(k)}$ denotes the peak powe in $K-th$ channel. The first term is the SPM and the second term denotes the contribution of XPM. In deriving Eq. (2.18), $P_0^{(k)}$ was assumed to be constant. In practice, time dependence of P_0 makes ϕ_{NL} to vary with time. In fact, the nonlinear optical phase shift changes with time in exactly the same fashion as the optical pulse due to SPM. It can be seen from Eq. (2.18), that the XPM induced phase shift is twice of SPM when the optical power of all of the channels are equal. XPM causes asymmetric spectral broadening of optical pulses, timing jitter and amplitude distortion in time domain.

The four wave mixing (FWM) is another effect that generates new frequency components. For WDM systems, with carrier frequencies of f_i, f_j and f_k the signal at new frequency $f_h = f_i + f_j - f_k$ can be generated by FWM, which leads to serious performance degradation when the newly generate frequency components fall into other WDM channels. For a single carrier systems, when the pulse have strong broadening due to chromatic dispersion, the nonlinear mixing of overlapped pulses generates ghost pulses in neighboring time slots due to intra-channel four wave mixing

(IFWM), which is one of the dominant penalties for high bit rate (above 40 Gb/s) fiber optic systems [11–13]. The difference between FWM and IFWM is that echo pulses appear in time domain instead of in frequency domain.

As far as transmission on fibre is concerned the non-linear effects are nearly always undesirable. After attenuation and dispersion, they provide the next major limitation on optical transmission. Indeed in some situations they are more significant than either attenuation or dispersion. A lot of research goes into suppressing the impairments induced by SPM, XPM and FWM for long haul and wideband fiber optic communication systems.

2.2 Coherent Transmission Technology

A coherent receiver linearly down-converts the optical signal to the electrical domain by using homodyne/heterodyne detection. A schematic diagram of a single branch coherent receiver is shown in Fig. 2.1. The basic idea of the coherent is that the received optical signal is mixed with a coherent local oscillator before it passes through a photo-detector.

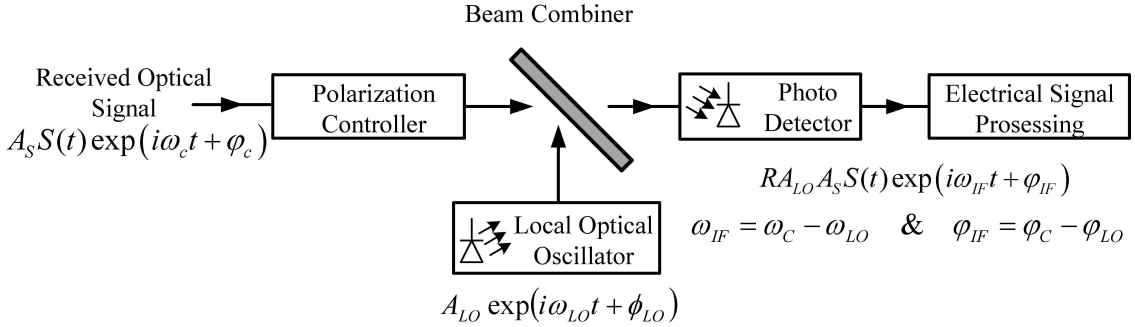

Figure 2.1: Schematic diagram of a coherent detection.

Suppose that the polarization of the received signal is perfectly aligned with that of the local oscillator (LO). The state of polarization of the received signal can be controlled using the polarization controller (PC). Let the transmitted signal be

$$E_T(t) = A_0 s(t) \exp(i\omega_c t) \tag{2.19}$$

Let us assume a perfect optical channel that introduces neither distortion nor noise. Only the phase of the optical carrier is changed due to propagation. Let the received signal after the PC be

$$E_R(t) = A_s s(t) \exp[i(\omega_c t + \phi_c)] \tag{2.20}$$

where $A_s s(t)$ is the complex received field envelope, ω_c is the optical carrier and ϕ is the phase. The electrical field of local oscillator is given by

$$E_{LO}(t) = A_{LO} \exp[i(\omega_{LO} t + \phi_{LO})] \tag{2.21}$$

These two signals are combined using a optical beam combiner and pass through a photo-detector (PD). The output electrical current of the PD is proportional to the absolute square of the incident optical field, and it can be written as

$$I(t) = R\left|\frac{q_S(t)}{\sqrt{2}} + \frac{q_{LO}(t)}{\sqrt{2}}\right|^2 = \frac{R}{2}|A_s s(t)|^2 + |A_{LO}|^2 + 2A_s A_{LO} Res(t) exp[i(\omega_{IF} t + \phi_c - \phi_{LO})] \tag{2.22}$$

where

$$\omega_{IF} = \omega_c - \omega_{LO} \tag{2.23}$$

is called the intermediate frequency. Typically, the LO output power, A_{LO}^2, is much

larger than the signal power, A_s^2, and therefore, the first term in Eq. (2.22) can be ignored. Since the LO output is continues wave, A_{LO}^2 is a constant and it leads to a DC component in the photo current, which can be removed by capacitive coupling. Therefore, the signal that goes to the front-end can be written as

$$I_d(t) = RA_sA_{LO}Res(t)exp[i(\omega_{IF}t + \phi_c - \phi_{LO})] \tag{2.24}$$

If $\omega_{IF} = 0$, such a receiver is known as homodyne receiver. Otherwise, it is called heterodyne receiver. For homodyne receiver, the phase of the received carrier ϕ_c should be exactly the same as the phase of the local oscillator ϕ_{LO}. This can be achieved using optical phase locked loop, or it can be post-corrected using the digital phase estimation techniques. When the phases are exactly aligned ($\phi_c = \phi_{LO}$), Eq. (2.24) can be written as

$$I_d(t) = I_0Re[s(t)] \tag{2.25}$$

where $I_0 = RA_sA_{LO}$. If the transmitted signal is real such as that corresponding to the amplitude modulated signal, the real part of $s(t)$ has all the information that is transmitted. If the transmitted signal is complex such as that corresponding to multilevel phase shift keying (MPSK) and quadrature amplitude modulation (QAM), phase diversity receivers are required to fully restore the transmitted information. The received signal and LO outputs are divided into two parts using power splitter (PS), and they are mixed together similar to what is done before. To recover the real part of $s(t)$, LO phase should be aligned with the optical carrier. Similarly, to recover the imaginary part of $s(t)$, the LO phase should be shifted by $\pi/2$, ($\exp(i\pi/2) = i$) with respect to optical carrier. Fig. 2.2 shows the block diagram of the single-branch

in-phase/quadrature coherent receiver, and as can be seen the phase information of optical carrier could be preserved using coherent detection.

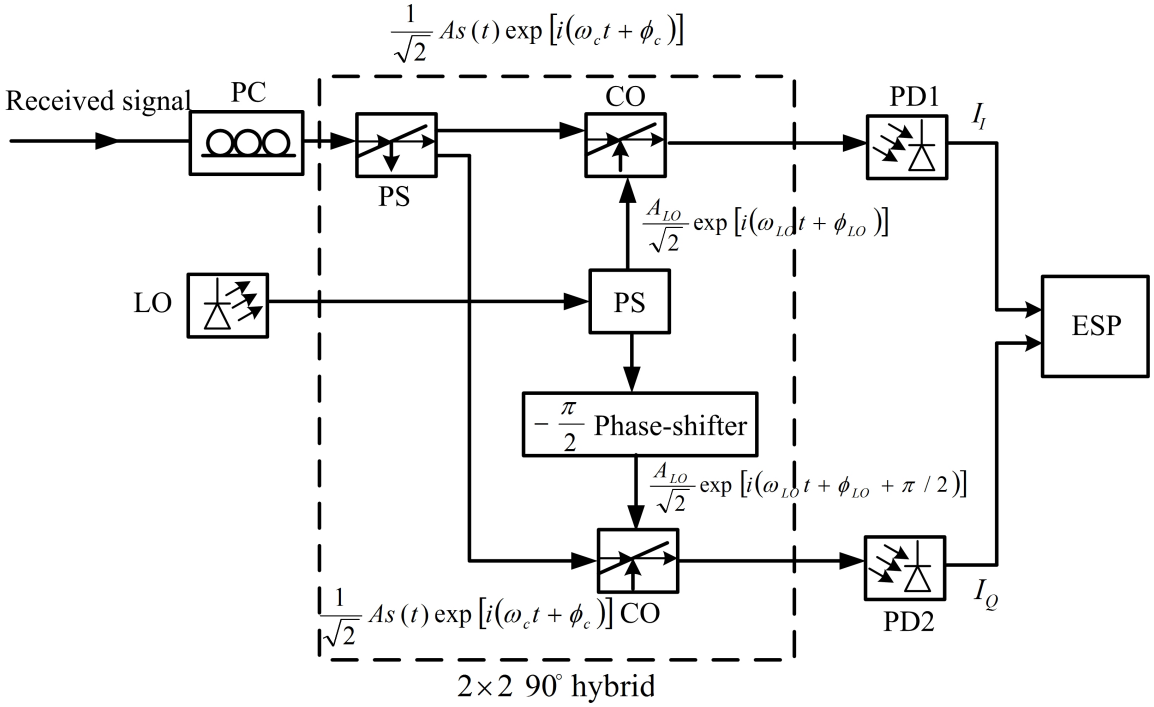

Figure 2.2: Schematic diagram of the single-branch in-phase/quadrature coherent receiver

For homo dyne detection, If the phase of the local oscillator is not fully aligned with the phase of the carrier, Eq. (2.24) can be written as

$$I_d(t) = I_0 Re[s(t) \exp(i\Delta\phi)], \tag{2.26}$$

where $\Delta\phi = \phi_c - \phi_{LO}$ is the phase error. If $\Delta\phi$ is $\pi/2$ and $s(t)$ is real, $I_d(t) = 0$, and therefore, the phase error leads to bit error. In contrast in heterodyne detection when, when local oscillator frequency $\omega_{LO} = 0$ is deviating from the received optical

carrier frequency $\omega_c = 0$. The optical signal first converted in to the microwave domain. Typically intermediate frequency is in the microwave or radio wave range and the resulting signal can be interpreted as the message $s(t)$ being modulated by the microwave or radio carrier of frequency ω_{IF}. It is because the microwave LO phase could be achieved using electrical phased locked loop (PLL), and therefore the optical PLL is no longer needed in heterodyne detection. However, this merit is gained at the cost of 3-dB penalty in the receiver sensitivity compared to homodyne detection. Recently, with the advent of high speed digital signal processors (DSPs), phase estimation can be done in digital domain for homodyne/heterodyne receivers, and therefore, analog PLL is no longer required. ,Advantage of homodyne detection is the optical receiver bandwidth (and also speed of A/D converter) is of order of symbol rate, B_s. In contrast for heterodyne detection, the receiver bandwidth should be $\sim 2B_s$ centered around ω_{IF}.

Since the coherent detection is linear in nature, the complex-valued electrical field with phase information can be achieved, and therefore, the amplitude, phase and frequency of the optical carrier can all be utilized to carry the information. There are several advantage for a coherent detection over a direct detection. First, the receiver sensitivity can be greatly improved by making the power of local oscillator sufficiently large. Second, the availability of higher-order modulation schemes in a coherent optical communication can further improve the spectral efficiency compared to conventional intensity modulation direct detection systems. Third, the heterodyne detection allow closely spaced WDM channels compared to that of direct detection systems. Last, the linearly detected signal by coherent detection enables the post signal processing in the electrical domain. Therefore, the electronic compensation

of chromatic dispersion (CD), polarization mode dispersion (PMD), and the fiber nonlinearity can be performed after the coherent detection using advanced DSP techniques. The combination of coherent detection and DSP is expected to become a very important transmission technique for the next generation of fiber optic communication systems due to its potential capacity and flexibility with various pre- and post-signal processing schemes in the electrical domain [14–22].

2.3 Dispersion Compensation Techniques

In fiber optic communication systems, information is transmitted over an optical fiber by using a coded sequence of optical pulses, whose width is set by the bit rate B of the system. Dispersion-induced broadening of pulses is undesirable as it interferes with the detection process, and it leads to errors if the pulse spreads outside its allocated bit slot ($T_B = 1/B$). Clearly, group velocity dispersion (GVD) limits the bit rate B for a fixed transmission distance L. The dispersion problem becomes quite serious when optical amplifiers are used to compensate for fiber losses because L can exceed thousands of kilometers for long-haul systems. The implementation of fiber dispersion compensation can be done at the transmitter, at the receiver or within the fiber link. In this section, several dispersion compensation techniques are discussed, and their advantage and disadvantage are also compared.

Before the development of high-speed powerful DSPs, conventional optical systems employ a dispersion management scheme that places a dispersion compensation module (DCM) at the amplifier site to negate the dispersion of the transmission link. The DCM compensates GVD while the amplifier takes care of fiber losses. A DCM

could be a dispersion compensating fiber (DCF) with the reverse sign of GVD parameters as that of the transmission fiber, or an optical filter with inverse transfer function of the fiber channel.

The use of DCF for dispersion compensation was first proposed in 1980, but due to the high loss of DCFs, this technique was not applied in practice until 1990s when the erbium-doped fiber amplifier (EDFA) was presented. A typical transmission fiber (TF) consisted of the standard single mode fiber (SSMF) with anomalous dispersion at 1550 nm and the DCF placed at the optical amplifier site within a double stage amplifier and it is shown in Fig 2.3.

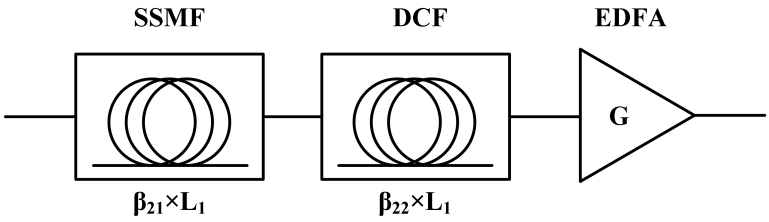

Figure 2.3: A transmission span with a DCF. β_{21}, L_1 and β_{22}, L_2 are the GVD parameter and length for SSMF and DCF, respectively

It can be shown that the total transfer function of SSMF cascades with a DCF is given by

$$H_{span}(\omega) = \exp\left[\frac{j\omega^2}{2}(\beta_{21}L_1 + \beta_{22}L_2)s(t)\right] \tag{2.27}$$

It is evident from Eq. (2.27), that the perfect dispersion compensation is realized if

$$\beta_{21}L_1 + \beta_{22}L_2 = 0. \tag{2.28}$$

Therefore, the optical pulses at the receiver are not broadened, and there is no ISI due

to dispersion. Since β_{21} is negative (anomalous GVD) for standard fibers, therefore DCF must have normal dispersion $\beta_{22} > 0$, such that the accumulated dispersion in Eq. (2.28) becomes zero. The DCF with large positive value of GVD have been developed for the sole purpose of dispersion compensation in order to keep L_2 as small as possible. The use of DCFs provides an all-optical technique that is capable of overcoming the detrimental effects of chromatic dispersion (CD) in optical fibers, provided the average signal power is low enough that the nonlinear effects remain negligible.

This scheme is quite attractive but suffers from two problems. First, insertion losses of a DCF module typically exceed 5 dB. Insertion losses can be compensated by increasing the amplifier gain but only at the expense of enhanced amplified spontaneous emission (ASE) noise. Second, because of a relatively small mode diameter of DCFs, the effective mode area is only $\sim 20\ \mu\text{m}^2$. As the optical intensity is large inside a DCF at a given input power, the nonlinear effects are considerably enhanced [23]. These two shortage limits the use of DCF in the long-haul fiber links.

Since the early 1990s, there has been great interest in using electronic equalizers as replacements for optical dispersion compensating modules at the receiver. Compared with the optical counterpart, the electronic dispersion compensation (EDC) has the advantages of lower cost and ease of adaption.

For a transmitter based dispersion compensation scheme, fiber dispersion can be canceled by pre-distorting the input pulses before they are launched in to the fiber link. Koch and Alferness presented a technique in 1985 to compensate fiber dispersion using the synthesis of pre-distorted signal [21]. The pre-chirped Gaussian pulse were obtained using a frequency modulated (FM) optical carrier as input to an external

modulator for amplitude modulation (AM). The output pulse is a chirped Gaussian pulse with the chirp parameter $C > 0$ such that $C\beta_2 < 0$ in a single mode optical fiber with typical $\beta_2 = -21$ ps^2/Km. The dispersion induced chirp is canceled out the intentionally induced chirp in the input pulses, and therefor, the pulse broadening is suppressed at the output of fiber. An alternative to implement signal pre-distortion is making use of DSP. With the advances in the performance of high-speed devices since 1990s, the signal pre-distortion can be done in electrical domain using DSP for the bit rate of 10 Gb/s and above in fiber optical transmission systems.

The disadvantage of pre-compensating scheme is that the exact dispersion compensation can not be achieved without the knowledge of the transmission fiber link. Furthermore, even if the transfer function of the fiber link is fully known, the optimum performance of the dispersion compensation is still hard to reach because in fiber link when an optical pulse propagate, other linear and nonlinear effects such as polarization mode dispersion and self phase modulation, interact with dispersion and change the pulse shape further and leading to lower performance of pre-compensation schemes. To avoid prior-knowledge of the fiber link setup requirement and achieve the optimum dispersion compensation, the dispersion compensation moved from the transmitter to the receiver and this schemes called dispersion post compensation or receiver based dispersion compensation.

There are several receiver-based EDC techniques. A linear equalizer can be used between the receiver and the detector to compensate for the ISI caused by fiber dispersion. A transversal filter (tapped delay line) is often used as a linear equalizer, and the weight coefficients can be adaptively adjust using well known least-mean square

(LMS) and zero-forcing (ZF) algorithms. For a conventional fiber optic communication system with direct detection, due to the power-law detection the linear EDC techniques discussed above can only partially undo the fiber dispersion because linear dispersion-induced distortion in optical domain becomes nonlinear in the electrical domain. Some nonlinear equalization techniques were therefore developed for direct detection.

For a fiber optic communication system with direct detection, the nonlinearity induced by power law of the photo-detector make the dispersion compensation scheme more complex and less efficient. With development of powerful digital signal processors (DSPs) during the 2000s, the difficulty in tracking the received optical carrier phase in an optical coherent receiver was overcomed by using digital carrier phase estimation circuit [24]. Hence, the coherent receiver combined with electronic dispersion compensation (EDC) using DSP has become more practical in past decade. Since the phase information of transmitted signal is preserved in the coherent systems, in the other words the complex valued electrical field is fully detected at the coherent receivers, more options are available in coherent optical systems compare to direct detection.

One of the most attractive advantage of the receiver-based EDC is that the fiber dispersion can be adaptively compensated either in frequency-domain or time-domain even without the knowledge of the transmission link, since the impairment introduced by power-law detection is absent in coherent receivers. With the rapidly increasing demand for the bandwidth, the fiber optic communication tends to transmit high bit-rate information data through multi-carriers and WDM systems and this will suffer from the distortion caused by higher-order dispersion effects due to its large

bandwidth. Therefore, the compensation of higher-order dispersion effects become more and more important in long-haul high-speed fiber-optic communication systems and it seems that receiver-based EDC going to be main dispersion compensation technique of future.

2.4 Backward Propagation

In high-speed wavelength division multiplexed (WDM) systems, the interaction of fiber nonlinearity and dispersion leads to many degrading effects, limiting the total capacity as well as the achievable transmission distance. Digital backward propagation (DBP) schemes have drawn significant research interest recently because of their ability to undo fiber linear and nonlinear impairments. Electronic backward propagation was first studied in 2007 by Killey et al. as a transmitter-based compensation method [19]. Since in the absence of coherent detection, manipulation of the field is only possible at the modulator. However, with the coherent detection, recovery of the received electric field enables receiver-based backward propagation, which was first studied in 2008 [25]. Receiver-based backward propagation has the advantage that it can ultimately be adaptive without the need for a feedback channel. The basic idea behind backward propagation (BP) can be understood from the governing equation of fiber propagation. The propagation of the electrical field envelope of an optical signal can be modeled by a scalar nonlinear Schrdinger equation (NLSE) in optical fiber [9]

$$\frac{\partial u}{\partial z} = \left[\hat{D} + \hat{N}\right] u, \tag{2.29}$$

where $\hat{D}$ denotes the linear operator given by

$$\hat{D} = -i\frac{\beta_2(z)}{2}\frac{\partial^2}{\partial t^2} + \frac{\beta_3(z)}{6}\frac{\partial^3}{\partial t^3} - \frac{\alpha(z)}{2} \tag{2.30}$$

and $\hat{N}$ is the nonlinear operator given by

$$\hat{N} = i\gamma(z)|u|^2, \tag{2.31}$$

where $\beta_2(z)$, $\beta_3(z)$, $\alpha(z)$ and $\gamma(z)$ are the profile of second-order and third-order dispersion coefficients, loss/gain and nonlinear coefficient, respectively. The NLSE is an invertible equation in absence of noise, and the transmitted signal can be exactly recovered by backpropagating the received signal through the inverse NLSE. If the sign of z reversed in Eq. (2.29) and the received signal is taken as the input signal, Eq. (2.29) can be written as

$$\frac{\partial u}{\partial z} = \left[-\hat{D} - \hat{N}\right] u, \tag{2.32}$$

which is equivalent to passing the received signal through a fictitious fiber having opposite-signed loss/gain, dispersion and nonlinearity coefficients. Therefore, the transmitted signal can be exactly recovered using this method. This technique is referred as *backward propagation*. Eq. (2.32) can be numerically solved using split-step Fourier method (SSFM) in DSP. The performance of this scheme is limited by noise and step size used in SSFM for backward propagation. In principle, in the absence of noise, BP can completely compensate both fiber dispersion and nonlinearity when the step size used to solve Eq. (2.32) is chosen small enough. However, when

the noise is present, the transmitted signal can not be completely recovered using backward propagation because BP-based schemes can not compensate for stochastic nonlinear impairments such as nonlinear phase noise. In fiber optic communication systems inline optical amplifiers change the amplitude of the optical field envelope randomly and fiber nonlinear effects such as self-phase modulation convert the amplitude fluctuations to phase fluctuations which is known as *nonlinear phase noise*. The computational cost in digital BP increase as the step size decreases, as a result, in practice the step size should be chosen large enough to make computational effort at transmitter/receiver affordable. BP has the advantage that it can be used to compensate for any higher order dispersion. BP also can be implemented digitally, either at transmitter/receiver or jointly at both. since backward propagation operates directly on the complex-valued field $u(z,t)$, this technique is universal, as the transmitted signal can have any modulation format or pulse shape, including multicarrier transmission using orthogonal frequency-division multiplexing (OFDM) with quadrature amplitude modulation (QAM). The compensation of fiber nonlinearity and dispersion using BP has been demonstrated to enable larger launch power and longer transmission distance in any fiber optic communication system. For this reason, a novel backward propagation technique using highly nonlinear fibers was proposed in this thesis for jointly compensation of fiber nonlinearity and linear effects in optical domain.

Chapter 3

Analysis of Nonlinear Phase Noise in Fiber-Optic Communication Systems

3.1 Introduction

The response of all dielectric materials to light becomes nonlinear under strong optical intensity and optical fiber has no exception. Due to the fiber Kerr effect, the refractive index of optical fiber increases with optical intensity, inducing intensity dependent nonlinear phase shift. The spontaneous emission of light is a phenomena which appears during the optical signal amplification. It is not correlated with signal and has an additive nature. In long-haul lightwave systems with lumped amplifiers placed periodically along the link, each amplifier adds noise caused by the amplified spontaneous emission (ASE) that propagates with the signal in multiple fiber sections. The nonlinear term in the NLS equation couples the ASE and signal, and therefore,

modifies the signal through the three nonlinear effects, self phase modulation (SPM), cross phase modulation (XPM) and four wave mixing (FWM).

Gordon and Mollenauer (1990) first showed that when optical amplifiers are used to periodically compensate for fiber loss, nonlinear phase noise is induced by the interaction of the fiber Kerr effect and optical amplifier noise, often called the Gordon-Mollenauer effect [26]. Here, nonlinear phase noise is induced by self phase modulation through the amplifier noise in the same polarization as the signal and within an optical bandwidth matched to the signal. Phase modulated optical signals, both phase shift keying (PSK) and differential phase shift keying (DPSK), carry information by the phase of an optical carrier. Added directly to the phase of a signal, nonlinear phase noise degrades both PSK and DPSK signals and limits the maximum transmission distance. Early literatures studied the spectral broadening induced by nonlinear phase noise [27–29]. The performance degradation due to nonlinear phase noise is assumed the same effect as that due to laser phase noise. However, the statistical properties of nonlinear phase noise are not the same as laser phase noise. The probability density function (PDF) of nonlinear phase noise is required for performance evaluation of a phase modulated signal with nonlinear phase noise. However, because of fiber nonlinearity, it is usually hard to obtain the exact expression for PDF of nonlinear phase noise but if the actual PDF is approximated by a Gaussian one can use variance in order to evaluate system performance. When the optical signal is periodically amplified by optical amplifiers, amplifier noise is unavoidably added to the optical signal. In long-haul optical communication systems, nonlinear phase noise is accumulated span after span and the accumulation of nonlinear phase noise is the summation of the contribution from each individual span. As a result the system

performance is dominated by nonlinear phase noise, rather than thermal and laser phase noise.

In addition to nonlinear phase noise, amplifier ASE noise also affects optical pulses and induces not only energy and phase fluctuations but also timing jitter by shifting each pulse in a random fashion from its original location within the bit slot. The physical origin of ASE-induced time jitter can be understood by noting that optical amplifiers affect not only the amplitude but also the phase of the amplified signal. Time-dependent variations in the optical phase shift the signal frequency from the carrier frequency by a small amount after each amplifier. Since the group velocity of an optical pulse depends on its carrier frequency, because of dispersion, the speed at which a pulse propagates through the fiber is affected by each amplifier in a random fashion. Such speed changes produce random shifts in the pulse position at the receiver and are responsible for the ASE-induced timing jitter.

In this chapter, we derive an analytical expression for electric field and variance of nonlinear phase noise in dispersion-managed coherent fiber optic system based on binary PSK using a perturbation theory. At the end of the chapter we validate our analytical results and show that the results are in good agreement with numerical simulation. We are also suggesting that our analytical expression for variance of nonlinear phase noise could be used as a design tool to optimize the various parameters such as launch power or pre- and post-dispersion compensation percentage of the coherent optical system.

3.2 Quasi-Linear Systems

In many occasions fiber link can be seen as a quasi-linear system, if transmitted power is well controlled such that the nonlinear effect of fiber is not too large. Our work is based on this assumption and the nonlinearity of a fiber can be described by first-order and second-order perturbation approximation. In quasi-linear systems, dispersive effects are much stronger than the nonlinear effects, and therefore, the fiber nonlinearity can be considered as a small perturbation on the linear system. Since the dispersive effects are dominant in quasi-linear systems, neighboring pulses overlap and this system is also known as strongly pulse overlapped system [13] or pseudo-linear system [30]. Fig. 3.1 shows the typical coherent fiber-optic transmission system based on binary PSK.

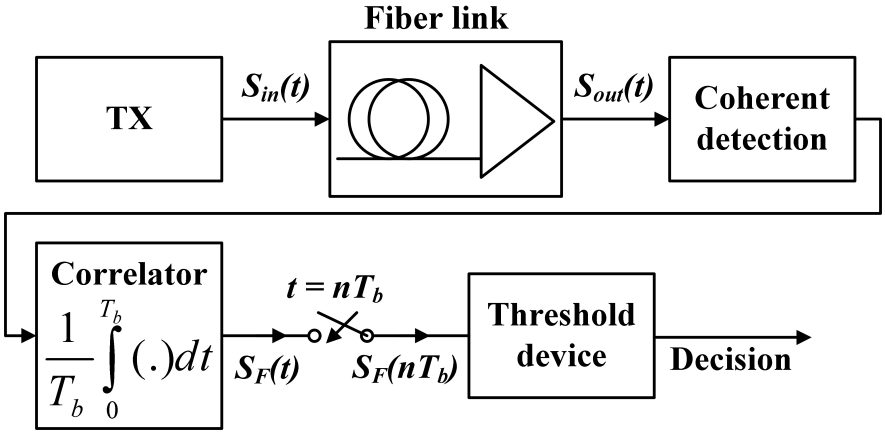

Figure 3.1: Schematic diagram of a coherent fiber optic system.

The optical field envelope in a fiber-optic transmission system can be described by the nonlinear Schrodinger equation (NLSE),

$$i\frac{\partial u}{\partial z} - \frac{\beta_2(z)}{2}\frac{\partial^2 u}{\partial t^2} - \frac{i\alpha}{2}u = -\gamma|u|^2u + iR(z,t) \tag{3.1}$$

where $\alpha(z)$ is the loss/gain profile which includes fiber loss as well as amplifier gain, $\beta(z)$ is the second-order dispersion profile and γ is the fiber nonlinear coefficient. $R(z,t)$ represents the noise field due to amplification, i.e.,

$$R(z,t) = \sum_{m=1}^{N_a} \delta(z - L_m) n^{(m)}(t), \tag{3.2}$$

where L_m is the location of an amplifier, N_a is the number of amplifiers, and $n^{(m)}(t)$ is the noise field due to an amplifier located at L_m. The mean and autocorrelation function of the noise field are given by

$$\langle n^{(m)}(t) \rangle = 0, \tag{3.3}$$

$$\langle n^{(m)}(t) n^{(m)*}(t') \rangle = \rho_m \delta(t - t') \tag{3.4}$$

and

$$\langle n^{(m)}(t) n^{(m)}(t') \rangle = 0, \tag{3.5}$$

where ρ_m is the amplified spontaneous emission (ASE) power spectral density (PSD) per polarization of an amplifier located at L_m The spectral density of spontaneous emission-induced noise is nearly constant (white noise) and can be written as [26]

$$\rho_m = n_{sp} h \overline{\nu} (G_m - 1), \tag{3.6}$$

where G_m is the gain of the amplifier, h is Planck's constant and, $\bar{v}$ is the mean optical carrier frequency. The parameter n_{sp} is called the spontaneous-emission factor (or the

population-inversion factor) and is given by

$$n_{sp} = \frac{N_2}{N_2 - N_1} \tag{3.7}$$

where N_l and N_2 are the atomic populations for the ground and excited states, respectively. We assume that the amplifier compensates for the fiber loss. To separate the fast variation of optical power due to fiber loss/gain, we use the following transformation [31],

$$q = \alpha(z)u, \tag{3.8}$$

and

$$\frac{\partial q}{\partial z} = \frac{\partial a}{\partial z}u + a\frac{\partial u}{\partial z}, \tag{3.9}$$

if

$$\frac{\partial a}{\partial z} = -\frac{\alpha(z)}{2}a. \tag{3.10}$$

Substituting Eqs. (3.9) and (3.10) in Eq. (3.1), we obtain

$$i\frac{\partial u}{\partial z} - \frac{\beta_2(z)}{2}\frac{\partial^2 u}{\partial t^2} = -\gamma a^2(z)\left|u\right|^2 u + iR(z,t). \tag{3.11}$$

Solving Eq. (3.9), we find

$$a(z) = \exp\left[-\int_0^z \frac{\alpha(s)}{2}ds\right]. \tag{3.12}$$

Between amplifiers, when the fiber loss is constant and Eq. (3.12) becomes

$$a(z) = \exp\left(-\alpha z/2\right). \tag{3.13}$$

Note that the mean optical power fluctuates due to fiber loss and amplifier gain, but $< |U(z)|^2 >$ is independent of distance since the variations due to loss/gain is represented by $a(z)$. Fig. 3.2 shows the typical dispersion and loss/gain profiles of a long-haul dispersion-managed fiber optic system. Eq. (3.11) can be solved using perturbation theory.

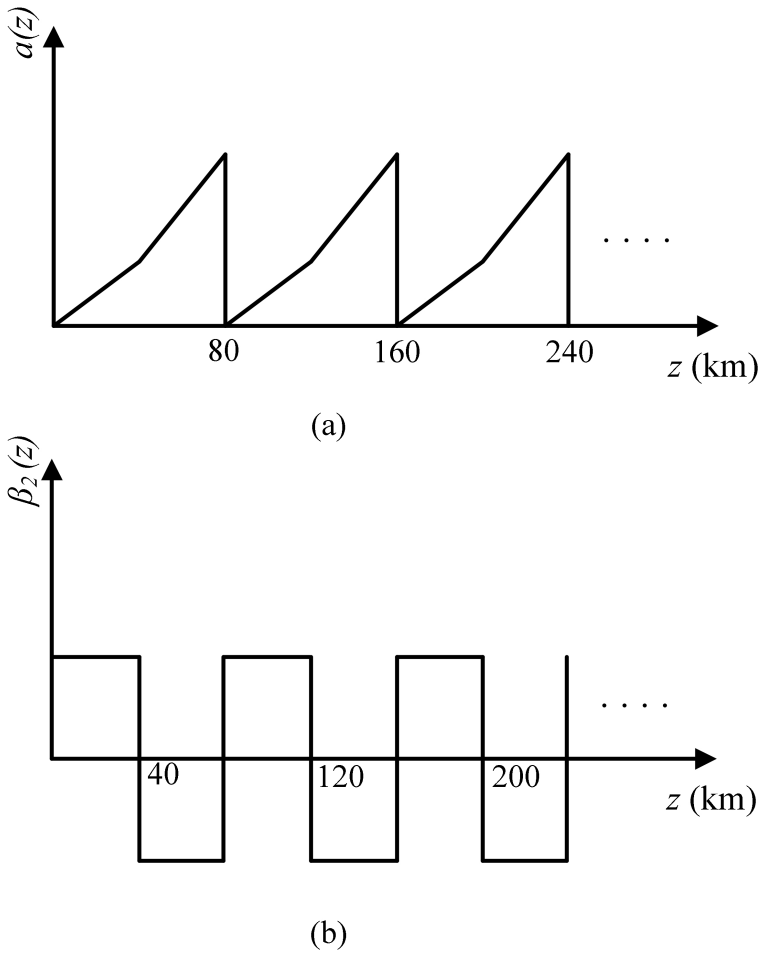

Figure 3.2: Typical dispersion and loss/gain profiles of a long-haul dispersion-managed fiber-optic system. Pre- and post- compensation are not shown.

The solution of Eq. (3.11) can be written as

$$u(t,z) = u_0(t,z) + \gamma u_1(t,z) + \gamma^2 u_2(t,z) + \cdots , \tag{3.14}$$

where $u_j(t,z)$ is the j-th order solution. Using Eq. (3.14), we find

$$|u(t,z)|^2 u(t,z) = \left| \sum_{n=0}^{\infty} \gamma^n u_n \right|^2 \sum_{n=0}^{\infty} \gamma^n u_n. \tag{3.15}$$

submitting Eq. (3.15) in Eq. (3.11) and separating terms proportional to $\gamma^n, \quad n = 0, 1, 2, \ldots$, we obtain

$$(\gamma^0): \qquad i\frac{\partial u_0}{\partial z} - \frac{\beta_2}{2}\frac{\partial^2 u_0}{\partial t^2} = 0, \tag{3.16}$$

$$(\gamma^1): \qquad i\frac{\partial u_1}{\partial z} - \frac{\beta_2}{2}\frac{\partial^2 u_1}{\partial t^2} = -a^2(z)\left|u_0\right|^2 u_0, \tag{3.17}$$

$$(\gamma^2): \qquad i\frac{\partial u_2}{\partial z} - \frac{\beta_2}{2}\frac{\partial^2 u_2}{\partial t^2} = -a^2(z)\left(2\left|u_0\right|^2 u_1 + u_0^2 u_1^*\right). \tag{3.18}$$

Eq. (3.16) is the linear Schrodinger equation. Eqs. (3.17) and (3.18) represent the first- and second-order corrections to the linear solution due to the nonlinear effects. When nonlinear effects are small, the terms of the order $\gamma^n, \quad n > 2$, can be ignored. Eq. (3.16) can be solved using the Fourier transform technique. The solution is

$$u_0(t,z) = \mathcal{F}^{-1}\left\{\widetilde{u}_0(\omega,0)\exp\left[i\omega^2 S(z)/2\right]\right\}, \tag{3.19}$$

where $\tilde{u}_0(\omega,0) = \mathcal{F}[u_0(t,0)]$, $u_0(t,0) = u(t,0)$ and $S(z)$ is the accumulated dispersion

$$S(z) = \int_0^z \beta_2(x)dx. \tag{3.20}$$

Eqs. (3.17) and (3.18) can also be solved using the same technique. Typically, in pseudo-linear systems, the nonlinear effects are smaller than dispersive effects and first order correction $u_1(t,z)$ is often adequate to describe the nonlinear propagation. However, when the transmission distance is long and/or launch power is large, second order perturbation theory is needed [32]. Therefore, in the next section, we derive an analytical expression for electric field and variance of nonlinear phase noise in dispersion-managed coherent fiber optic system based using a second-order perturbation theory.

3.3 Mathematical Derivation of Nonlinear Phase Noise Variance

In this section, we derive the variance of nonlinear phase noise for the received phase shift keying signals in a coherent fiber optic system. In the absence of nonlinear effects and amplifier noise, if a Gaussian pulse is launched to the fiber, its propagation is given by Eq. (3.19)

$$u_0(z,t) = u_{lin}(z,t) = \sqrt{E}F(z,t), \tag{3.21}$$

and

$$F(z,t) = \left[\frac{p(z)}{\sqrt{\pi}}\right]^{1/2} \exp\left\{-\frac{[p^2(z)+iC(z)]t^2}{2} + i\theta_0(z)\right\} \tag{3.22}$$

This appendix A.1 provides details of the calculation and E is pulse energy, $p(z)$, $C(z)$ and $\theta_0(z)$ are the inverse pulse width, chirp and phase factor, respectively, and

they are given by

$$p(z) = \frac{T_0}{\sqrt{T_0^4 + S^2(z)}}, \qquad C(z) = \frac{S(z)p^2(z)}{T_0^2} \tag{3.23}$$

$$\theta_0(Z) = \frac{1}{2}tan^{-1}[\frac{S(z)}{T_0^2}]. \tag{3.24}$$

Here, T_0 is the half-width at $1/e$ intensity point, and $S(z)$ is the accumulated dispersion given by Eq. (3.20). The peak power, P and energy, E are related by

$$P = \frac{E}{T_{eff}} \tag{3.25}$$

where $T_{eff} = \sqrt{\pi}T_0$, and $F(z,t)$ is normalized such that

$$\int_{-\infty}^{+\infty} |F(z,t)|^2 dt = 1 \tag{3.26}$$

Solving Eqs. (3.17) and (3.20) using the Fourier transform technique for a single Gaussian pulse, the first-order and second-order nonlinear correction terms can be found as

$$u_1(z,t) = \gamma|E|\sqrt{E}g^{(1)}(z,t)F(z,t), \tag{3.27}$$

and

$$u_2(z,t) = \gamma^2|E|^2\sqrt{E}g^{(2)}(z,t)F(z,t), \tag{3.28}$$

where $g^{(1)}(z,t)$ and $g^{(2)}(z,t)$ can be found as

$$g^{(1)}(z,t) = j\frac{T_0^2}{\sqrt{\pi}}\int_0^z \frac{\exp(-a(s) - \Delta(s)t^2)}{T_1(s)|T_1^2(s)|\sqrt{\delta(z,s)R(s)}}ds \tag{3.29}$$

and

$$g^{(2)}(z,t) = -2g_x^{(2)}(z,t) + g_y^{(2)}(z,t) \tag{3.30}$$

where

$$g_x^{(2)}(z,t) = \frac{T_0^3}{\pi}\int_0^z\int_0^s \frac{\exp(-a(s+s') - \Delta_x(s)t^2)}{T_1(s')|T_1^2(s')||T_1^2(s)|\sqrt{\delta(s,s')R(s')}} \times \frac{dsds'}{\sqrt{\delta_x(s,s',z)R_x(s,s')}} \tag{3.31}$$

and

$$g_y^{(2)}(z,t) = \frac{T_0^3}{\pi}\int_0^z\int_0^s \frac{\exp(-a(s+s') - \Delta_x(s)t^2)}{T_1^*(s')|T_1^2(s')|T_1^2(s)\sqrt{\delta^*(s,s')R^*(s')}} \times \frac{dsds'}{\sqrt{\delta_y(s,s',z)R_y(s,s')}} \tag{3.32}$$

where $T_1^2 = T_0^2 - iS(z)$ and $\Delta(s)$, $\Delta_k(s,s',z)$ $k = x, y$, $\delta(z,s)$, etc are given by Kumar et. al. [32] (Appendix A.2), where a second-order perturbation theory was developed for self phase modulation (SPM).

Now, consider the optical field envelope immediately after an amplifier located at L_m. The optical field envelope in the absence of amplifier noise can be written as

$$u(L_m,t) = \sqrt{E}\sum_{j=0}^{+\infty}\gamma^j|E|^j g^{(j)}(L_m,t)F(L_m,t). \tag{3.33}$$

In this section, we study the combined effect of SPM and amplifier noise using the second-order perturbation theory. For the analytical treatment of the problem, we approximate the field given by Eq. (3.33) with best-fitting Gaussian pulse, which is in the form of

$$u(L_m,t) \simeq \sqrt{E_m}F(L_m,t), \tag{3.34}$$

where

$$\sqrt{E_m} = \int_{-\infty}^{+\infty} u(L_m, t) F^*(L_m, t) dt. \tag{3.35}$$

Here $\sqrt{E_m}$ is a complex electrical field amplitude which takes into account the first-order and second-order nonlinear effects.

Focusing only on the impact of the noise added by this amplifier, the optical field envelope at L_{m+} can be written as

$$u(L_{m+}, t) = \sqrt{E_m} F(L_m, t) + n(t), \tag{3.36}$$

where $n(t) \equiv n^{(m)}(t)$ is the noise field added by the amplifier at L_m. In this section, we consider only two noise modes given by

$$n(t) = (n_{0r} + i n_{0i}) F(L_m, t) \tag{3.37}$$

where $n_{0r} = \mathrm{Re}\{n_0\}$, and $n_{0i} = \mathrm{Im}\{n_0\}$ are the amplitudes of the in-phase and quadrature components of the noise field added by the amplifier at L_m, respectively, and n_0 is the complex amplitude of the noise field. The analysis of nonlinear phase noise with higher order noise modes (arbitrary DOF) have been carried out in Ref. [33], and the result show that the impact of higher order noise is negligible for distances of practical interest. Substituting Eq. (3.37) in Eq. (3.36), we find

$$u(L_{m+}, t) = (\sqrt{E_m} + n_0) F(L_m, t) \tag{3.38}$$

Thus, the complex amplitude of the field envelope has changed because of the amplifier noise. Treating Eq. (3.38) as the initial condition, the zeroth-order (i.e. linear) optical

field envelope is described by

$$u^{(0)}(z,t) = (\sqrt{E_m} + n_0)F(z,t), \quad z > L_m \tag{3.39}$$

In practical systems operating in the pseudo-linear regime, the dispersion of the transmission fibers is fully compensated at the receiver either in optical or electrical domain. i.e. $S(L_{tot}) = 0$, and therefore, $F(L_{tot}, t) = F(0, t)$. Solving Eqs. (3.17) and (3.18) with the zeroth order solution given by Eq. (3.39) and the condition $S(L_{tot}) = 0$, the total field envelope at the end of the transmission line is

$$\begin{aligned} u(L_{tot},t) &= (\sqrt{E_m} + n_0) \times \sum_{j=0}^{+\infty} \gamma^j |\sqrt{E_m} + n_0|^{2j} g^{(j)}(L_{tot},t) F(L_{tot},t) \\ &= (\sqrt{E_m} + n_0) \times \sum_{j=0}^{+\infty} \gamma^j |\sqrt{E_m} + n_0|^{2j} g^{(j)}(L_{tot},t) F(0,t) \end{aligned} \tag{3.40}$$

where $g^{(0)}(z,t) = 1$, and $g^{(j)}(z,t)$, $j = 1, 2$ are given by Eqs. (3.29) and (3.30).

The output of in-phase-quadrature (IQ) coherent receiver has two output currents which are proportional to real and imaginary parts of the optical field envelope. For simplicity, we assume that the constant of proportionality to be unity, since it does not affect the performance of a long-haul fiber-optic system. The output of the IQ receiver passes through the digital signal processing (DSP) unit after A/D converter and arbitrary filter shapes can be realized using DSP. We assume that the output of the IQ receiver passes through a matched filter, or equivalently a correlator and the

decision is based on the correlator output

$$\begin{aligned} u_f &= \int_{-\frac{T_s}{2}}^{+\frac{T_s}{2}} u(L_{tot},t)F^*(0,t)dt \\ &\simeq \int_{-\infty}^{+\infty} u(L_{tot},t)F^*(0,t)dt \end{aligned} \tag{3.41}$$

where T_s is the symbol interval. Substituting Eq. (3.40) in Eq. (3.41) and keeping the terms up to second-order in γ, we find

$$u_f = (\sqrt{E_m} + n_0)\sum_{j=0}^{+2} \gamma^j |\sqrt{E_m} + n_0|^{2j} g_f^{(j)}, \tag{3.42}$$

where

$$g_f^{(j)} = \int_{-\infty}^{+\infty} g_f^{(j)}(L_{tot},t)F^*(0,t)dt. \tag{3.43}$$

The phase of the correlator output is

$$\phi = \tan^{-1}\left[\frac{Im\{u_f\}}{Re\{u_f\}}\right] = \phi_d + \delta\phi_m \tag{3.44}$$

where ϕ_d is deterministic phase change due to self phase modulation in the absence of amplified spontaneous emission (ASE), and $\delta\phi_m$ is the stochastic phase change due to ASE of amplifier located at L_m and signal due to SPM. $\delta\phi_m$ can be divided into three parts,

$$\delta\phi_m = \delta\phi_m^{(0)} + \delta\phi_m^{(1)} + \delta\phi_m^{(2)} \tag{3.45}$$

where $\delta\phi_m^{(0)}$ is the linear phase change due to ASE, $\delta\phi_m^{(1)}$ and $\delta\phi_m^{(2)}$ are the first- and second-order nonlinear phase changes due to ASE and SPM interaction, respectively.

They can be calculated as

$$\delta\phi_m^{(0)} = \frac{1}{\sqrt{E_{mr}}} n_{0i} + \frac{\sqrt{E_{mi}}}{E_{mr}} n_{0r}, \tag{3.46}$$

$$\delta\phi_m^{(1)} = 2\gamma\sqrt{E_{mi}}\; g_{fr}^{(1)} n_{0i} + 2\gamma\sqrt{E_{mr}}\; g_{fr}^{(1)} n_{0r} \tag{3.47}$$

and

$$\begin{aligned}\delta\phi_m^{(2)} &= 4\gamma^2|E_m|\sqrt{E_{mi}}\;\{g_{fr}^{(2)} - g_{fr}^{(1)} g_{fi}^{(1)}\} n_{0i} \\ &+ 4\gamma^2|E_m|\sqrt{E_{mr}}\;\{g_{fr}^{(2)} - g_{fr}^{(1)} g_{fi}^{(1)}\} n_{0r}\end{aligned} \tag{3.48}$$

where $g_{fr}^{(j)}(z) = \mathrm{Re}\{g_f^{(j)}(z)\}$ and $g_{fi}^{(j)}(z) = \mathrm{Im}\{g_f^{(j)}(z)\}$, where $j = 0, 1, 2$ and $n_{0r} = \mathrm{Re}\{n_0\}$ and $n_{0i} = \mathrm{Im}\{n_0\}$. In Eqs. (3.47) and (3.48), we have ignored terms proportional to γ^3, n_{0r}^2, n_{0i}^2 and $n_{0r}n_{0i}$. Variance of phase noise can be easily found by squaring Eq. (3.45), and averaging the noise terms using Eqs. (3.3) to (3.5), we obtain [34]

$$\begin{aligned}\langle\delta\phi_m^2\rangle = \frac{\rho_m}{2}\Bigg\{ &\frac{1}{\sqrt{E_{mr}}} + 2\gamma\sqrt{E_{mi}}\; g_{fr}^{(1)} \\ &+ 4\gamma^2|E_m|\sqrt{E_{mr}}\;[g_{fr}^{(2)} - g_{fr}^{(1)} g_{fi}^{(1)}]\Bigg\}^2 \\ &+ \frac{\rho_m}{2}\Bigg\{ \frac{\sqrt{E_{mi}}}{E_{mr}} + 2\gamma\sqrt{E_{mr}} g_{fr}^{(1)} \\ &+ 4\gamma^2|E_m|\sqrt{E_{mr}}\;[g_{fr}^{(2)} - g_{fr}^{(1)} g_{fi}^{(1)}]\Bigg\}^2.\end{aligned} \tag{3.49}$$

Eq. (3.45) provides variance of the phase noise that includes both first-order and second-order nonlinear effects and derivation of this equation is the main contribution of this chapter.

Since the noise of amplifiers are statistically independent, variance of phase noise due to all the amplifiers is

$$\langle \delta\phi^2 \rangle = \sum_{m=1}^{Na} \langle \delta\phi_m^2 \rangle \tag{3.50}$$

For M-ary PSK signals, symbol error probability is determined solely by the probability density function (PDF) of the phase. Under the Gaussian PDF assumption, the variance calculated from Eq. (3.50) can be related to the symbol error probability for BPSK signals [23, 35]. Eq. (3.50) is valid for arbitrary dispersion map when the dispersion of the transmission fibers is fully compensated either at the transmitter, receiver or inline (i.e. $S(L_{tot} = 0)$).

3.4 Numerical Simulations and Result

To test the accuracy of the perturbation theory, numerical simulation of the NLS equation is carried out using the symmetric split-step Fourier scheme (SSFS) [9]. The main idea of SSFS is to separate the linear and nonlinear part of the NLS equation. More specifically, propagation from z to $z + h$ is carried out in two section, in the middle of which the nonlinearity is lumped. In the middle, the nonlinearity acts separately while in the neighboring sections, dispersion and absorption acting alone. Schematic illustration of symmetric SSFS is given in Fig. 3.3.

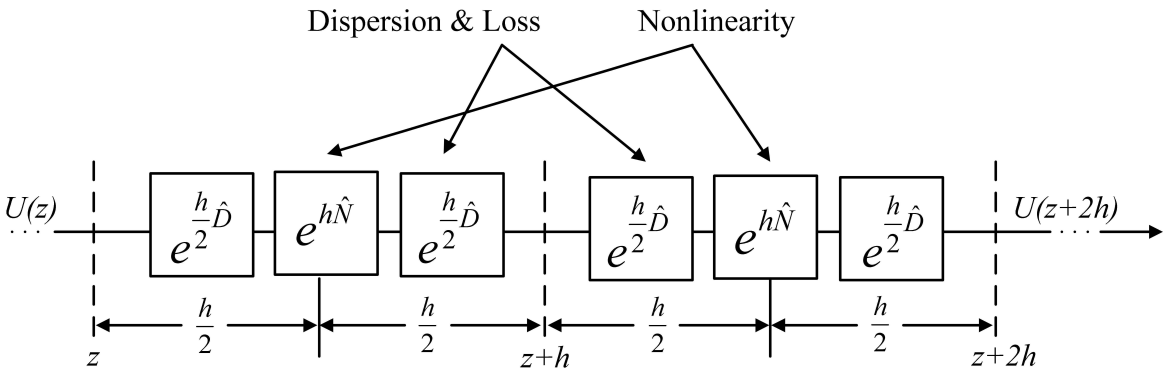

Figure 3.3: Schematic illustration of symmetric-SSF scheme

In Section 2.4, we have seen that NLS equation can be written as

$$\frac{\partial u}{\partial z} = \left[\hat{D} + \hat{N}\right] u, \tag{3.51}$$

where

$$\hat{D} = -i\frac{\beta_2(z)}{2}\frac{\partial^2}{\partial t^2} + \frac{\beta_3(z)}{6}\frac{\partial^3}{\partial t^3} - \frac{\alpha(z)}{2} \tag{3.52}$$

$$\hat{N} = i\gamma(z)|u|^2 \tag{3.53}$$

In SSFS, for the linear part, $\hat{D}$, fast Fourier transform (FFT) is employed, and for the nonlinear operator $\hat{N}$, the ordinary differential equation can be solved analytically, if the step size is chosen small enough such that the nonlinear term can be assumed to be constant. Therefore, the analytical solution of Eq. (3.51) can be approximate as

$$u(z+h,t) = \exp\left(\frac{h}{2}\hat{D}\right)\exp\left(h\hat{N}\right)\exp\left(\hat{D}\frac{h}{2}\right)u(z,t) \tag{3.54}$$

3.4.1 Variance of Nonlinear Phase Noise

In this section, we implement the simulation based on analytical phase noise variance given by Eq. (3.49) and also Monte-Carlo simulation to verify the result from the analytical formula. 8192 runs of NLS equation are carried out and the phase variance of the decision variable is calculated in Monte-Carlo simulation. The lumped amplification is assumed throughout this chapter. The critical simulation parameters are listed in Table 3.1.

Table 3.1: Simulation parameters.

Bit rate	40 Gb/s
Pulse width (FWHM)	7.5 ps
Pulse shape	Gaussian
Peak power (P_0)	2 dBm
Spontaneous-emission factor (n_{sp})	1
Amplifier spacing (L_{span})	80 Km
Transmission distance (L_{tot})	2400 Km
Num. of NLS runs in Monte-Carlo sim.	8192
Computational bandwidth	320 GHz

We consider a dispersion-managed fiber-optic system with two segments. The first segment is a standard anomalous dispersion fiber and this is followed by a reversed dispersion fiber of equal length and the same absolute dispersion. The fiber loss α and nonlinear coefficient γ for both of the fibers are 0.2 dB /Km and 2.43 $W^{-1}Km^{-1}$, respectively. Spontaneous-emission factor n_{sp} is equal to 1 which corresponds to a

noise figure (NF) of 3 dB. Matched filter is used in electrical domain at the end of the transmission line in the receiver and no optical filter is used.

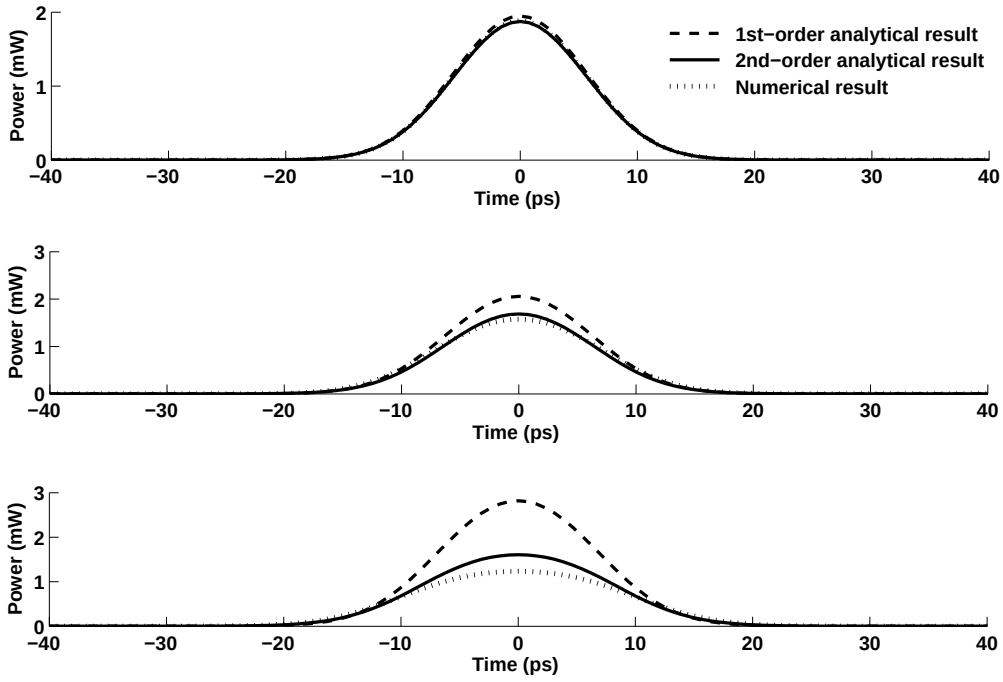

Figure 3.4: Optical power as a function of time at total transmission distance of (a) 160 Km, (b) 480 Km and (c) 960 Km. The dotted, broken, and solid lines show the numerical, first-order, and second-order solution, respectively. $|D| = 4$ ps/nm.Km.

Fig. 3.4, shows the optical power as a function of time at different total transmission distance calculated using Eqs. (3.27) and (3.28). The peak power is 2 mW and absolute value of dispersion is 4 ps/nm.Km. It can be seen from Fig. 3.4 at large transmission distance, the first-order perturbation theory becomes inaccurate. However, results of second-order perturbation theory is in good agreement with numerical simulations.

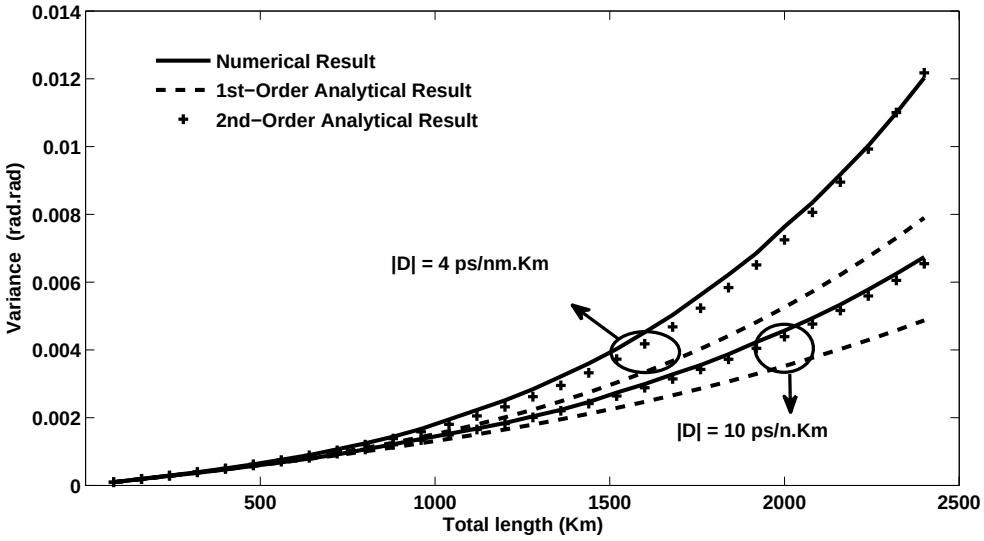

Figure 3.5: Phase variance dependence on the total length of the transmission line.

In Fig. 3.5 the '-' and '+' marks show the phase variance calculated using the first- and second-order analytical perturbation theory, respectively and the solid line shows the numerical simulation results. As the dispersion increases, the variance of nonlinear phase noise due to SPM decreases consistent with the results of [36, 37]. The nonlinear phase variance grows cubically with distance [33] and, therefore, the difference between the variances for the case of $|D| = 4$ ps/nm.Km and $|D| = 10$ ps/nm.Km increases significantly for longer transmission lengths. In long transmission lengths, as can be seen, there is a discrepancy between the first-order analytical results and numerical simulation results. However, results of second-order perturbation theory is in good agreement with numerical simulations.

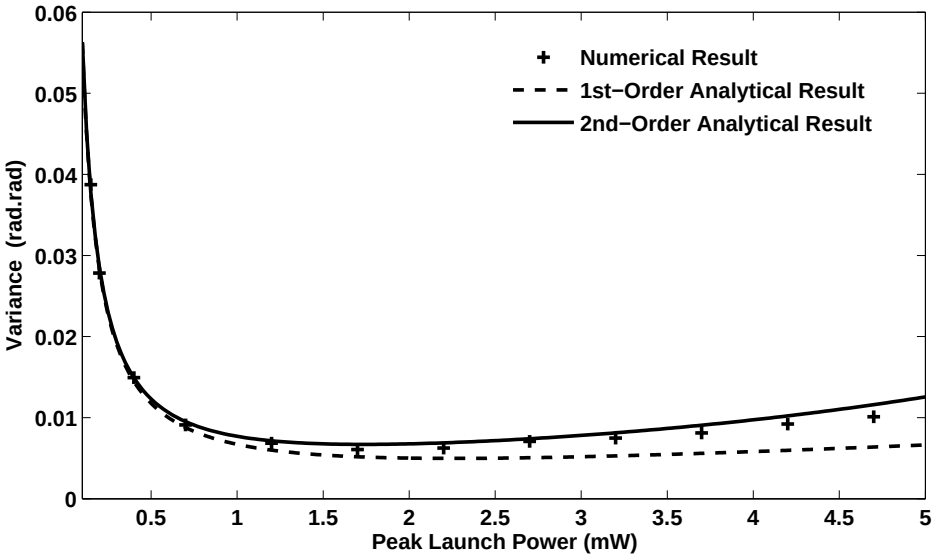

Figure 3.6: Dependence of phase variance on peak launch power. $L_{tot} = 2400$ Km and $|D| = 10$ ps/nm.Km

Fig. 3.6, shows the dependence of phase variance versus the launch power at total transmission distance of 2400 Km and $|D| = 10$ ps/nm.Km. When the launch power is low, the linear phase noise dominates (because of dependence $1/E$). At high launch power, nonlinear phase noise becomes significant (because of E dependence). At large launch powers, the first-order perturbation theory is known to become inaccurate. However, as can be seen, results of second-order perturbation theory is in good agreement with numerical simulations.

3.4.2 Optimizing Dispersion-Managed Fiber-Optic Systems

Fig. 3.7 shows the fiber link CONSIST of pre-, post- and inline dispersion compensation.

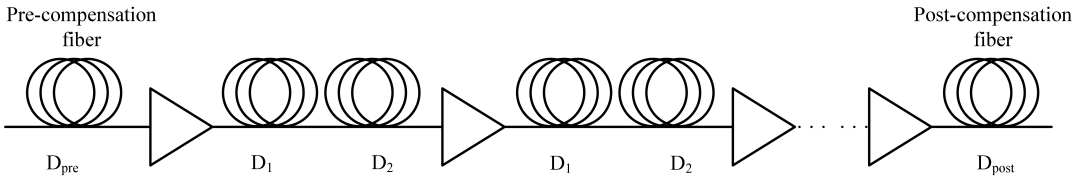

Figure 3.7: Dispersion-managed fiber link with pre- and post-dispersion compensation.

As we mentioned before the variance calculated using Eq. (3.50) can be related to the symbol error probability for PSK signals and it is valid for arbitrary dispersion maps when the dispersion of the transmission fibers is fully compensated either at the transmitter/receiver or inline (i.e. $S(L_{tot}) = 0$). Therefore our analytical formula can be used to optimized such systems. Fig. 3.8, shows the dependence of phase variance on the launch power at total transmissin distance of 2400 Km and $|D| =$ 10 ps/nm.Km using analytical and numerical methods. As can be seen in Fig. 3.8 the phase noise variance become minimum at $P = 1.6$ mW which corresponds to minimum bit error rate power.

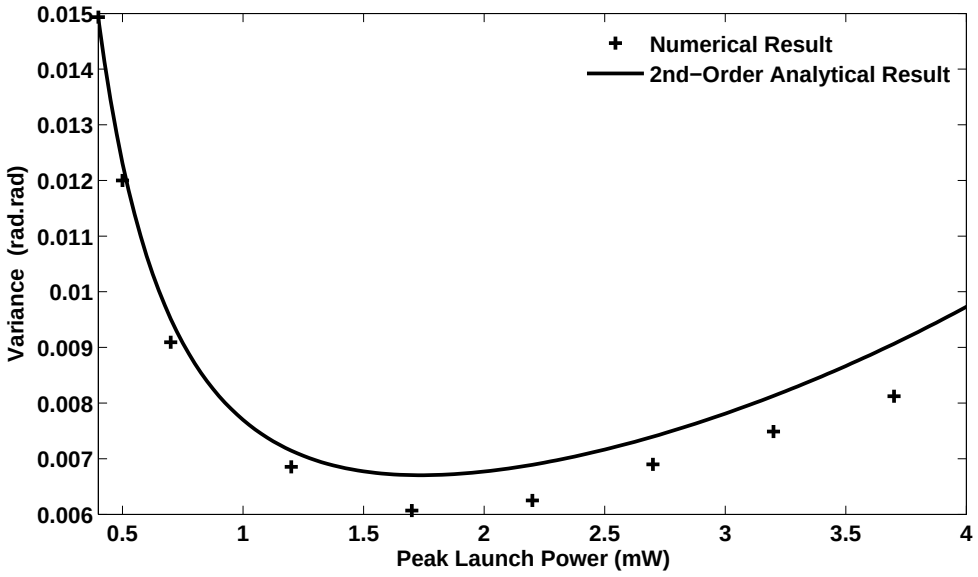

Figure 3.8: Dependence of phase variance on peak launch power. $L_{tot} = 2400$ Km and $|D| = 10$ ps/nm.Km

The numerical simulation of NLS equation is time consuming, however, the analytical method based on solving NLS equation using perturbation approximation is quite efficient and therefore the analytical variance can be obtained more easily without requiring extensive computational efforts, and also with fairly good accuracy for quasi-linear systems.

3.5 Conclusion

We have developed analytical expressions for the linear and nonlinear phase noise variance due to SPM using second-order perturbation theory. It is found that as the transmission reach and/or lunch power increase, the variance of the phase noise calculated using first order perturbation theory becomes inaccurate. However, the

variance calculated using second order perturbation theory is in good agreement with numerical simulations. We have also showed that the analytical formula derived in this chapter for the variance of nonlinear phase noise can be used as a design tool to investigate the optimum system design parameters such as power and dispersion maps for dispersion-managed coherent fiber optic systems based on phase shift keying.

Chapter 4

Optical Back Propagation for Fiber Optic Communications Using Highly Nonlinear Fibers

4.1 Introduction

Backward propagation (BP) schemes have drawn significant research interest recently because of their ability to undo fiber linear and nonlinear impairments [20, 33, 38]. In principle, BP schemes could undo the deterministic (bit-pattern dependent) nonlinear impairments, but it can not compensate for the stochastic nonlinear impairments such as nonlinear phase noise. Inline optical amplifiers change the amplitude of the optical field envelope randomly and fiber nonlinear effects such as self phase modulation (SPM) convert the amplitude fluctuations to phase fluctuations which is known as nonlinear phase noise. The impact of nonlinear phase noise was first studied in Ref. [26] for dispersion-free fiber-optic systems. Refs. [37] and [39] have found that the

fiber dispersion lowers the impact of nonlinear phase noise. When the BP schemes are used, deterministic nonlinear impairments such as self phase modulation (SPM), cross phase modulation (XPM) and four wave mixing (FWM) can be suppressed and therefore. stochastic nonlinear impairments such as nonlinear phase noise could become dominant. The analysis of nonlinear phase noise is given in chapter 3 where an analytical expressions for the linear and nonlinear phase noise variance using second-order perturbation theory is calculated.

In this chapter, we investigate two types of backward propagation (BP) schemes. The first scheme is the digital BP (DBP) in which the distortions due to fiber dispersion and nonlinear effects can be undone by solving the nonlinear Schrodinger equation (NLSE) in digital domain with the sign of distance being reversed. The DBP improves the transmission performance significantly. However, it requires considerable amount of computational resources, and therefore, currently transmission experiments have used DBP only in off-line signal processing. The second scheme is optical BP (OBP) which could undo the fiber dispersion and nonlinear effects in optical domain. The OBP module is placed at the end of the fiber optic link which consists of dispersion compensating fibers (DCF) and nonlinearity compensators (NLC). NLC imparts a phase shift that is equal in magnitude to the nonlinear phase shift due to fiber propagation, but opposite in sign.

In this chapter, we also introduce a novel inline optical nonlinearity compensation technique which incorporate inline optical nonlinear compensators and dispersion compensating fibers at receiver. We will show that the in line nonlinearity compensation has better performance than OBP and DBP schemes.

4.2 Theoretical Background on Backward Propagation

The signal propagation along a fiber is governed by nonlinear Schrodinger equation (NLSE) [9] in the loss less form

$$\frac{\partial u}{\partial z} = -i\frac{\beta_2}{2}\frac{\partial^2}{\partial t^2} + \frac{\beta_3(z)}{6}\frac{\partial^3}{\partial t^3} + i\gamma(z)a^2(z)|u|^2u, \tag{4.1}$$

or

$$\frac{\partial u}{\partial z} = \left[\hat{D} + \hat{N}\right]u, \tag{4.2}$$

where $\hat{D}$ and $\hat{N}$ denote the linear and nonlinear operators, receptively, which are given by

$$\hat{D} = -i\frac{\beta_2}{2}\frac{\partial^2}{\partial t^2} + \frac{\beta_3(z)}{6}\frac{\partial^3}{\partial t^3} \tag{4.3}$$

$$\hat{N} = i\gamma(z)a^2(z)|u|^2 \tag{4.4}$$

where β_2, β_3 and γ are the second-order and third-order dispersion coefficients and nonlinear coefficient, respectively and

$$a^2(z) = \exp[-\mathrm{mod}(z, L_{span})\alpha] \tag{4.5}$$

Here α is the fiber loss/gain coefficient and L_{span} is the amplifier spacing (i.e. the fiber span length between amplifiers). For simplicity, we have assumed that the fibers in the link are identical and amplifier spacing is uniform and fiber loss is fully compensated after each span by erbium doped fiber amplifiers (EDFAs). Eq. (4.1) can be numerically solved using split-step Fourier method (SSFM). The solution of

Eq. (4.1) is given by

$$u(t, L) = Mn(t, 0) \tag{4.6}$$

where

$$M = \exp\left\{\int_0^{L_{tot}} [D(z) + N(z)]dz\right\} \tag{4.7}$$

Here, L_{tot} is the total transmission distance. The distortions caused by dispersion and nonlinearity, can be undone by means of digital signal processing (DSP) or an optical back propagation module (OBM). Suppose we multiply Eq. (4.6) by M^{-1}, we obtain

$$u(t, 0) = M^{-1}u(t, L_{tot}) \tag{4.8}$$

Since $\exp(x)\exp(-x) = 1$ for any operator x. it follows that

$$M^{-1} = \exp\left\{-\int_0^{L_{tot}} [D(z) + N(z)]dz\right\} \tag{4.9}$$

which is equivalent to solving the following partial differential equation

$$\frac{\partial u}{\partial z} = -\left[\hat{D} + \hat{N}\right] u, \tag{4.10}$$

with the initial condition $u(t, L_{tot})$. Since Eq. (4.10) can be obtained by reversing the spatial variable z in Eq. (4.1), this technique is referred to as backward propagation.

4.2.1 Digital Backward Propagation

Digital back propagation (DBP) is a technique which could undo the fiber dispersion and nonlinear effects in electrical domain at the receiver. In DBP, fiber transmission process is entirely reversed using fictitious fiber in digital domain with parameters (

i.e. α, β_2, β_3 and γ) with opposite sign of the transmission fiber to recover initial signal. The amplifier with gain G is replaced by an attenuator with loss G.

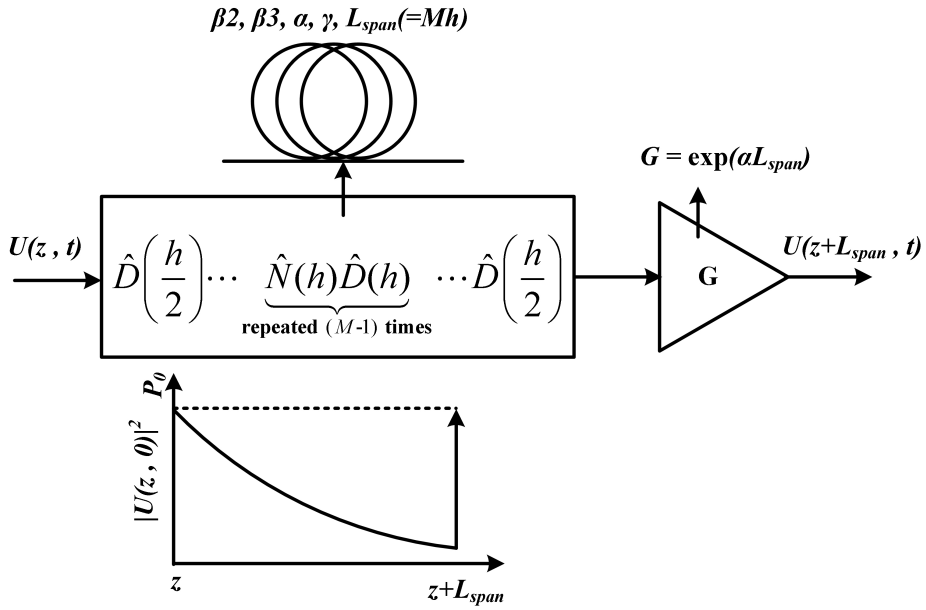

Figure 4.1: Symmetric split-step Fourier method (SSFM) used to simulate the signal forward propagation through the transmission fiber.

Typically, the NLSE is solved in electrical (digital) domain with the above parameters using the conventional symmetric SSFS, which is shown in Fig. 4.1. The length of each fiber span is divided into M small segments of step size, h. Smaller h gives better performance, but leads to more extensive calculation efforts. At the receiver, after the coherent detection, the received signal with complex field envelope passes through a DBP compensator implemented using DSP. An ideal DBP compensator is shown in Fig. 4.2. In this work. we will discuss two types of DBP.

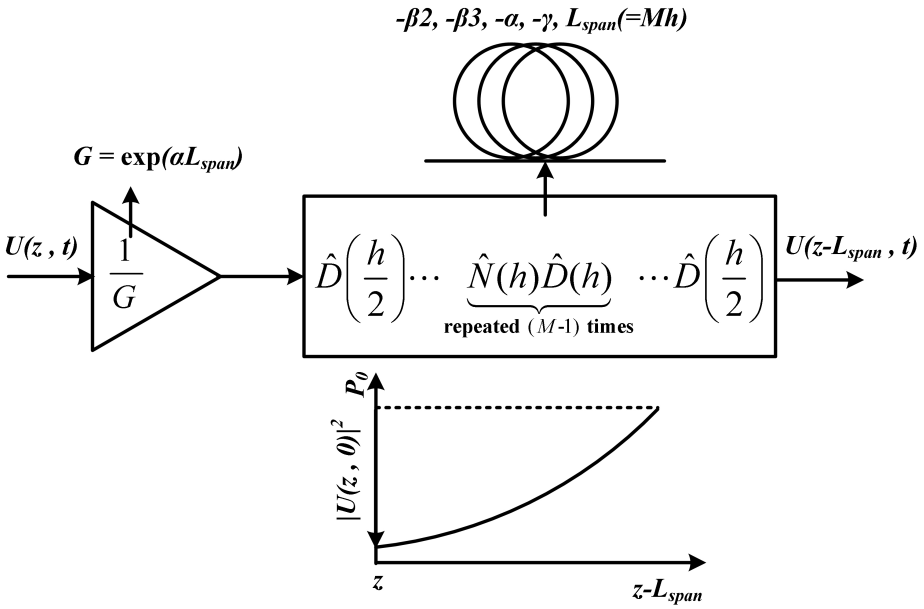

Figure 4.2: An ideal backward propagation for a single span.

For type 1. the DBP has step size equal to amplifier spacing, called AS-DBP, and for type 2, very small step size (same step size as that used in forward propagation) is used in BP. We call this perfect DBP. In this chapter. the NLSE is solved using the non-iterative symmetric SSFM, and its corresponding forward propagation mathematical expression for one fiber span is given by [9],

$$u(z+h,t) = \exp\left(\frac{h}{2}\hat{D}\right) exp\left(\int_z^{z+h} \hat{N}(\tau)d\tau\right) \exp\left(\frac{h}{2}\hat{D}\right) u(z,t) \tag{4.11}$$

Note that, at the end of each span, the gain $G = \exp(\alpha L_{span})$ is applied. The mathematical expression of backward propagation therefore can be written as

$$u(L_{tot}-(z+h),t) = \exp\left(-\frac{h}{2}\hat{D}\right) exp\left(\int_z^{L+(z+h)} \hat{N}(\tau)d\tau\right) \exp\left(-\frac{h}{2}\hat{D}\right) u(L_{tot}-z,t) \tag{4.12}$$

where L_{tot} is the total transmutation distance. One of the disadvantages of the ideal DBP is that computational complexity increases significantly as h decreases. In Ref. [143], it is proposed to use asymmetric split-step Fourier scheme step size equal to amplifier spacing (AS-DBP) and with a variable parameter to optimize the BER. The AS-DBP can be realized as [40, 41],

$$u_1(z+h,t) = u(L-z,t)\exp\left(-i\eta\gamma|u(L-z,t)|^2 L_{eff}\right), \tag{4.13}$$

where

$$\tilde{u}(L_{tot}-(z+L_{span}),\omega) = \tilde{u}(z,\omega)\exp\left(-i\left[\frac{\beta_2}{2}\omega^2+\frac{\beta_3}{6}\omega^3\right]L_{span}\right), \tag{4.14}$$

$$L_{eff} = \frac{1-\exp(-\alpha L_{span})}{\alpha}, \tag{4.15}$$

α is the fiber loss coefficient, $\tilde{u}(z,w)$ is the Fourier transform of $u_l(z,t)$ and η is the variable parameter to be optimized to increase the performance. In the case of AS-DBP. the computational complexity increases linearly with the number of spans.

4.2.2 Optical Backward Propagation

Optical back propagation (OBP) is a technique which could undo the fiber dispersion and nonlinear effects in optical domain using optical back propagation module instead of electrical domain [42]. The optical back propagation module consists of dispersion compensation fibers and nonlinear compensators. A nonlinear compensator uses two highly nonlinear fibers (HNFs) to compensate the nonlinearity of the transmission fiber. At the end of the fiber optic link, an optical back propagation module (OBP)

is placed as shown in Fig. 4.3a.

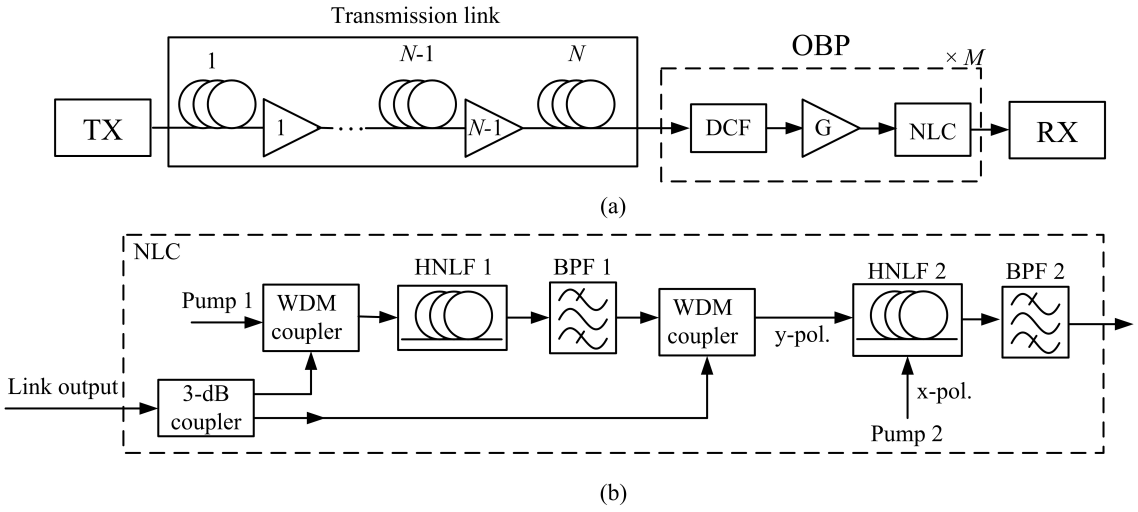

Figure 4.3: (a) Block diagram of a fiber-optic link with optical back propagation. (b) Block diagram of NLC.

Let the input of OBP module be the output of fiber optic link. In order to recover the initial field envelope at the output of OBP, the transfer function of the OBP should be the inverse of that of the fiber-optic link M^{-1} given by Eq. (4.9). To realize M^{-1}, we utilize the symmetric split-step Fourier technique with step size of h [9],

$$M^{-1} \approx A(t, 0, h/2)B(t, h)A(t, h/2, 3h/2)B(t, 2h) \dots B(t, L_{tot})A(t, L_{tot} - h/2, L_{tot}) \tag{4.16}$$

where

$$A(t, x, y) = \exp\Big(- iD(t)(y - x)\Big) \tag{4.17}$$

and

$$B(t,x) = \exp\left(- i \int_{x-h}^{x} a^2(z)|u(t,z)|^2 dz \right). \tag{4.18}$$

Here, $A(t,x,y)$ represents the fiber dispersive effects over the interval $[x\ y]$ and $B(t,x)$ represents the nonlinear phase shift accumulated over a fiber length h at x. Typically, the function $a^2(z)$ varies more rapidly than $|u(t,z)|^2$, and therefore, in the interval $[x-h\ x]$, $|u(t,z)|^2$ can be approximated to be independent of z, i.e. $|u(t,z)|^2$, $|u(t,x)|^2$ and now, the integral in Eq. (4.18) can be evaluated analytically using Eq. (4.5) as

$$B(t,x) = \exp\left(- i\gamma h_{eff} \exp[-mod(x, L_{span})\alpha]|u(t,x)|^2 \right) \tag{4.19}$$

where

$$h_{eff} = \frac{m[1-\exp(-\alpha L_a)]}{\alpha} + \frac{1-\exp[-\mathrm{mod}(h, L_{span})\alpha]}{\alpha}, \tag{4.20}$$

with $m = floor(h/L_{span})$. When the step size is equal to amplifier spacing, Eq. (4.19) reduces to Eq. (4.13) i.e. AS-DBP, for simplicity we assume that the step-size is an integral multiple of the amplifier spacing, i.e., $h = mL_{span}$, m being an integer. The operator B takes the form

$$B(t,x) = \exp\left(-i\gamma \frac{m[1-\exp(-\alpha L_{span})]}{\alpha} |u(t,x)|^2 \right). \tag{4.21}$$

The operator A can be realized using a dispersion compensating. fiber (DCF) as shown in 4.3a. The first DCF of OBP compensates for the half of the accumulated dispersion of the last span of the fiber optic link assuming that the step size is equal to the amplifier spacing. The launch power to DCF is low, so that nonlinear effects in DCF can be ignored. An amplifier is introduced to compensate for the loss in

DCF. If there exists a fiber with negative nonlinear coefficient, the operator B can be easily realized through self phase modulation (SPM) in such a fiber. Unfortunately, such a fiber is not available. Here, it is proposed to realize the operator B using a nonlinearity compensator (NLC) whose schematic is shown in Fig. 4.3b. First the output signal of the fiber-optic link, u_s $(= u(t, L_{tot})/\sqrt{2})$ and a CW pump beam (pump 1) of frequency Ω (relative to optical carrier frequency) are launched into a highly nonlinear fiber HNLF1. The field envelope of the pump beam after propagating a distance L_1 in a dispersion-free HNLF1 is given by [9]

$$u_{p1}(t, L_1) = u_{p1}(t, 0) \exp\Big(i2\gamma_1 L_{eff,1}|u_s(t)|^2 + i\theta_1 + i\Omega t\Big), \tag{4.22}$$

where $L_{eff,1}$ and γ_1 are the effective length and nonlinear coefficient of HNLF1, respectively and $\theta_1 = \gamma_1 L_{eff,1}|u_{p1}(t, 0)|^2$. In Eq. (4.22), the first and second terms on the exponent represent the XPM and SPM, respectively. L_{ef} and γ_1 are so chosen that the nonlinear phase shift due to XPM is equal in magnitude to the phase shift given by Eq. (4.21), but of opposite sign,

$$\gamma_1 L_{eff,1} = -\gamma \frac{m[1 - \exp(-\alpha L_s pan)]}{\alpha}. \tag{4.23}$$

The signal u_s and the pump beam at the output of HNLF1 are multiplexed using a WDM coupler and its output is launched into a highly nonlinear fiber HNLF2. A second CW pump beam, pump 2 that has the same frequency as pump 1 is launched into HNLF2. The polarization of pump 2 is chosen to. be orthogonal to signal polarization. Typically, highly nonlinear fibers are birefringent fibers and the field

envelope of pump 2 at the output of HNLF2 is given by [9]

$$u_{p2}(t,L_2) = u_{p2}(t,0)\exp\left(\frac{i2\gamma_2 L_{eff,2}|u_s(t)+u_{p1}(t,L_1)|^2}{3} + i\theta_2 + i\Omega t\right), \qquad (4.24)$$

where $L_{eff,2}$ and γ_2 are the effective length and nonlinear coefficient of HNLF2, respectively, and $\theta_2 = \gamma_2 L_{eff,2}|u_{p2}(t,0)|^2$. As before, first and second terms on the exponent of Eq. (4.24) represent the XPM and SPM effects, respectively. We choose the nonlinear coefficient γ_2, effective length $L_{eff,2}$, powers of signal and pump 1 such that the phase shift due to XPM in HNLF2 is quite small,

$$2\gamma_2 L_{eff,2}|u_s(t)+u_{p1}(t,L_1)|^2/3 \ll \pi. \qquad (4.25)$$

Under these conditions, Eq. (4.24) can be approximated as

$$\begin{aligned} u_{p2}(t,L_2) &\approx u_{p2}(t,0)\left(1+\frac{i2\gamma_2 L_{eff,2}|u_s(t)+u_{p1}(t,L_1)|^2}{3}\right)\exp\big(i(\theta_2+\Omega t)\big) \\ &\approx u_{p2}(t,0)\exp(i\theta_2)\Bigg\{\frac{1+2i\gamma_2 L_{eff,2}(|u_s|^2+|u_p(t,0)|^2)}{3}\exp\big(i\Omega t\big) \\ &+ \frac{2i\gamma_2 L_{eff,2}u_s u_{p1}^{\star}(t,0)}{3}\exp\Big(-i2\gamma_1 L_{eff,1}|u_s(t)|^2 - i\theta_1\Big) \\ &+ \frac{2i\gamma_2 L_{eff,2}u_s^{\star}u_{p1}(t,0)}{3}\exp\Big(i2\gamma_1 L_{eff,1}|u_s(t)|^2 + i\theta_1 + 2i\Omega t\Big)\Bigg\}. \qquad (4.26) \end{aligned}$$

The first, second and third terms on the right hand side of Eq. (4.26) correspond to optical signals centered around Ω, 0 and 2Ω, respectively. If we introduce an optical band pass filter (OBF) with its center frequency at zero and bandwidth equal to the bandwidth of u_s (which is much smaller than Ω), frequency components centered

around Ω and 2Ω will be rejected by OBF. Therefore, the output of OBF is

$$u_{out} = K u_s(t) \exp\left(-i2\gamma_1 L_{eff,1}|u_s(t)|^2\right) \tag{4.27}$$

where $K = i2\gamma_2 L_{eff,2} u_{p2}(t,0) u_{p1}^*(t,0) \exp[i(\theta_2 - \theta_1)/3]$ is a complex constant. Thus, the phase shift provided by the OBP is of the form given by Eq. (4.21) which is required for back propagation. The phase of K is a constant and it has no impact on direct detection systems. When coherent detection is employed, this phase shift is removed by digital signal processing (DSP) unit of the coherent receiver.

4.2.3 Inline Optical Nonlinearity Compensation Scheme

Inline optical nonlinearity compensation (IONC) is a novel technique which could effectively undo the nonlinear effects in optical domain similar to OBP. This technique divides optical back propagation module to two parts, unlike OBP which has both nonlinear and linear compensators at receiver, it uses optical nonlinear compensators distributed throughout the fiber link before each amplifier to compensate for each span nonlinearity and therefore, makes the system efficiently linear. Dispersion compensation fiber (DCF) at the end of fiber link (i.e. receiver) to combat fiber linear effect. In the next section, we will see that this scheme can outperform both OBP and DBP techniques and gives the system longer reach and better tolerance to nonlinearity.

4.3 Results and Discussion

We have simulated a $N-$span fiber-optic transmission system without inline pre- and post-dispersion compensation in optical domain. Table 4.1 shows the system parameters listed in our simulation. For perfect-BP very small step size is chosen so that nonlinear phase does not exceed 0.0005 rad. A pseudo-random bit sequence (PRBS) of length 262144 is used in the simulations. The symbol rate is 25 GSym/sec, modulation format = 32 quadrature amplitude modulation (QAM). We assume that the coherent receiver is ideal and mainly focus on the impairments caused by dispersion and nonlinearity. Backward propagation provides equalization for both linear and nonlinear impairments, and therefore, no other equalizer is used.

Table 4.1: Simulation parameters.

Symbol rate	25 GSym/sec
Modulation format	32-QAM
Pulse shape	Gaussian
Transmission fiber dispersion (β_2)	-21 $W^{-1}Km^{-1}$
Transmission fiber loss (α)	0.2 dB/Km
Transmission fiber nonlinear coefficient (γ)	1.1 $W^{-1}Km^{-1}$
Amplifier spacing (L_{span})	80 Km
Spontaneous-emission noise factor (n_{sp})	1.5
Computational bandwidth	320 GHz

The numerical simulations of optical back propagation module and inline optical nonlinearity compensation are carried out with the following parameters: dispersion of DCF = -130 ps^2/Km, loss of DCF = 0.4 dB/Km, nonlinear coefficient of DCF = 4.2 $W^{-1}Km^{-1}$, nonlinear coefficient of HNLF1 fiber, γ_{HNLF1} = 2000 $W^{-1}Km^{-1}$, effective length of HNLF1 = 232 m, pump 1 power = 10 mW, frequency of the pump 1 (and also pump 2), n = 400 GHz, the full bandwidth of the optical band pass filters = 87.5 GHz. When the product of effective length and nonlinear coefficient of HNLF2 is large, the linear approximation done in Eq. (4.4.26) for XPM breaks down leading to performance degradations. On the other hand, if the product is too low, NLC would not compensate for transmission fiber nonlinear effects. Therefore, we have optimized the fiber parameters of HNLF2 to obtain the best transmission performance. The nonlinear coefficient γ_{HNLF2} and effective length of HNLF2 are chosen as 1000 $W^{-1}Km^{-1}$ and 200 m, respectively, and power of pump 2 = 5.625 mW. When the step-size is equal to amplifier spacing, effective length of HNLF1 = 232 m. When the step-size is twice the amplifier spacing, the effective length is doubled so that the nonlinear phase shift accumulated over two spans can be compensated. It may be possible to design the OBP module with all the NLC units sharing the same pump.

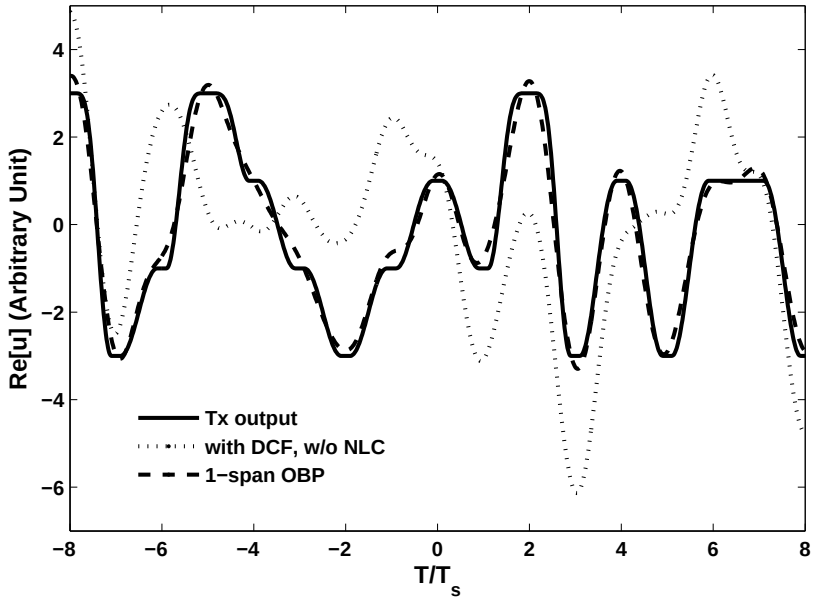

Figure 4.4: Optical field envelope vs normalized time. T_s = symbol interval, transmission distance = 800 Km, peak launch power to fiber-link = 0 dBm and n_{sp} = 0.

Fig. 4.4 shows the real part of the optical field envelope for different cases. The amplifier noise is turned off to see clearly the distortions due to fiber nonlinear effects. The solid and broken lines show the field envelopes at the transmitter output and OBP output, respectively. The dotted line shows the field envelope at the receiver with DCF and without NLC. As can be seen, the field envelope with OBP is closer to the transmitter output than that in the case, with DCF and without NLC.

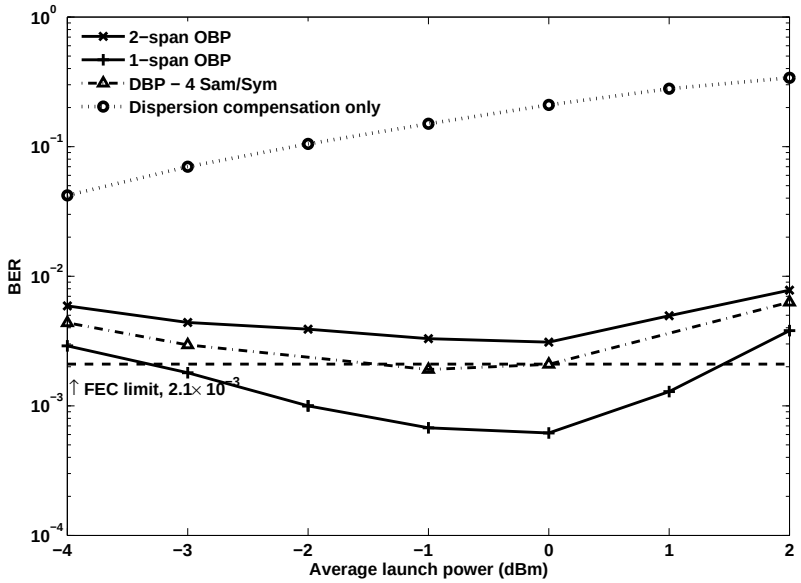

Figure 4.5: Bit error rate vs average launch power to the fiber-optic link. Transmission distance = 800 Km.

Fig. 4.5 shows the bit error rate (BER) as a function of transmission fiber launch power. Solid lines show the cases of optical backward propagation with step-size equal to L_{span} (1-span OBP) and step size equal to $2L_{span}$ (2-span OBP). The dotted and broken line shows the cases when NLC is absent and when digital backward propagation is used to compensated linear and nonlinear effects in fiber optic transmission system. As can be seen, OBP improves the performance significantly and 1-span OBP outperforms 2-span OBP and DBP.

4.3.1 Optical BP Vs. Digital BP

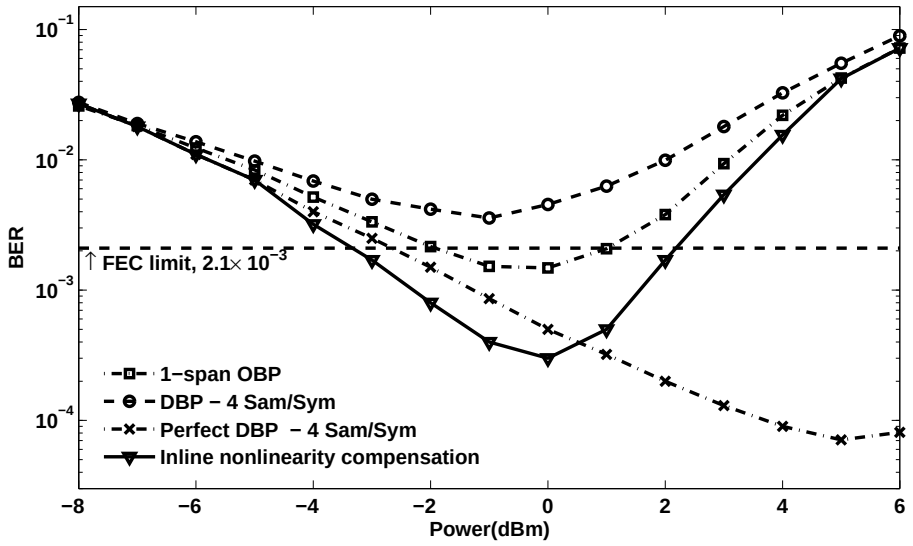

Figure 4.6: Bit error rate vs average launch power to the fiber-optic link for DBP, perfect-DBP, OBP and inline nonlinearity compensation.

Fig. 4.6 shows the BER as a function of average launch power to the fiber optic link for the DBP, perfect-DBP, OBP and inline nonlinearity compensation for transmission distance of 1040 Km. As can be seen, the perfect-DBP has the best performance among other schemes. In our simulations we have find out that perfect-DBP has reach of 46 span i.e. 3680 Km which is due to the fact that it is using very small step size to solve inverse NLSE which can undo the fiber nonlinearity and dispersion effects very effectively, but on the other hand it requires huge computational cost and as a result, it can not be used in current off-line signal processing because its large delay. Therefore, in practical systems, DBP step size is chosen to be equal to amplifier spacing (typically 80 Km), i.e. AS-DBP should be used. As can be seen from Fig. 4.6,

OBP and inline optical nonlinearity compensation can out perform AS-DBP while inline optical nonlinearity compensation has the best performance between this three schemes.

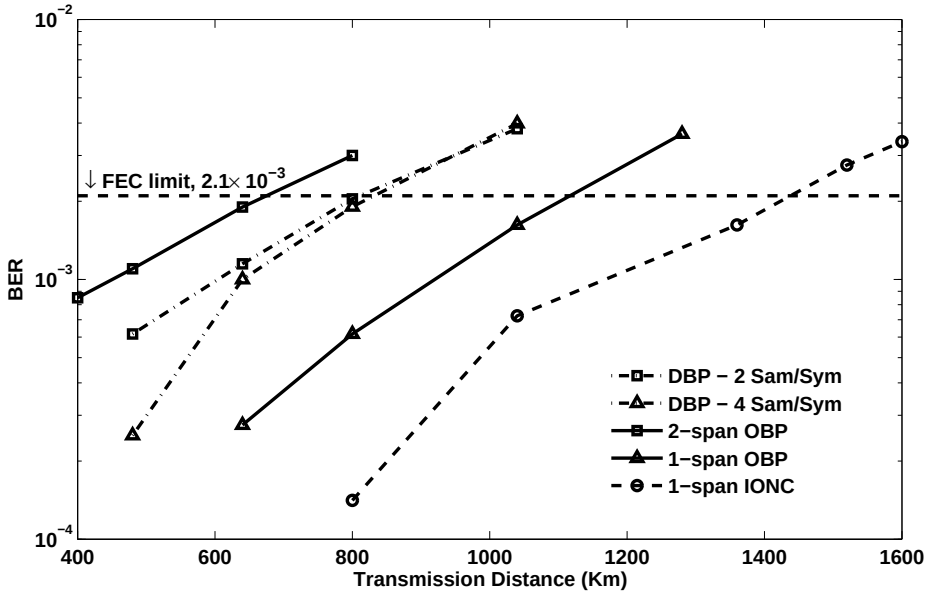

Figure 4.7: Bit error rate vs transmission reach for DBP, perfect-DBP, OBP and inline nonlinearity compensation (IONC).

Fig. 4.7 shows the .BER as a function of transmission reach. Each point in Fig. 4.7 is obtained after optimizing the launch power. The transmission reach without OBP, DBP and inline nonlinearity compensation (but with DCF) is limited to 240 Km at the forward error correction (FEC) limit of 2.1×10^{-3}. This is because the multi-level QAM signals are highly sensitive to fiber nonlinear effects. The maximum reach can be increased to 640 Km, 1040 Km and 1440 Km using 2-span OBP, 1-span OBP and inline optical nonlinearity compensation, respectively and in the case of perfect-DBP and AS-DBP maximum reach can be increased to 3680 Km and 800

Km, respectively.

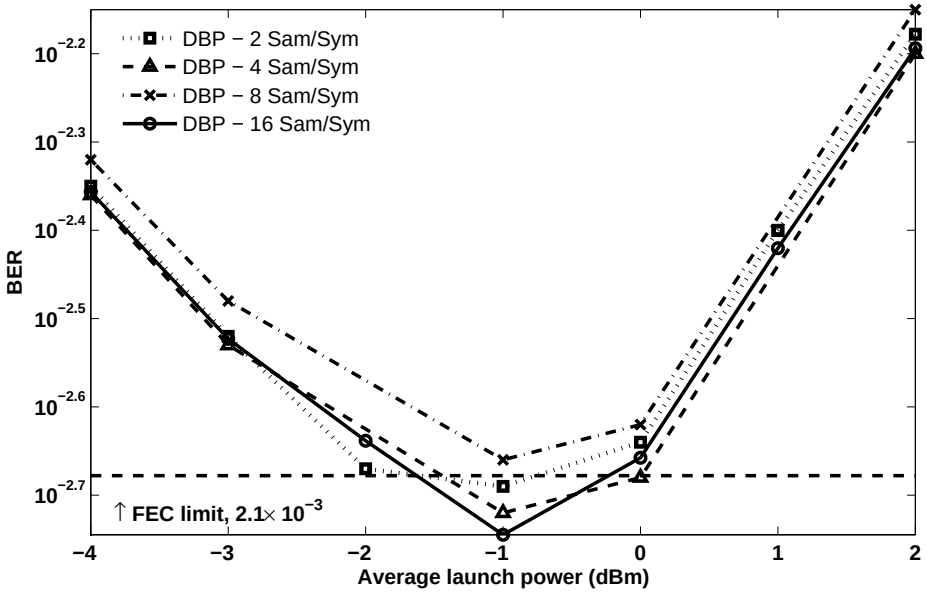

Figure 4.8: Bit error rate vs average launch power to the fiber-optic link for DBP schemes with 2, 4, 8, 16 sample per symbol.

Fig. 4.8 shows the BER as a function of average launch power to the fiber optic link for DBP schemes with 2, 4, 8, 16 samples per symbol when Transmission distance is equal to 800 Km. In Fig. 4.8 we find that the performance of 1-span DBP is almost the same for all of the cases and by increasing the number of samples per symbol in DBP we can not increases performance. 1-span OBP and AS-DBP is sharing the same basics in dispersion and nonlinearity compensation in the other word both of them are are realizations of split step Fourier method, while 1-span OBP has infinite number of samples per symbol (analog in time) therefore, the performance improvement in 1-span OBP could not be because of its analog nature OBP.

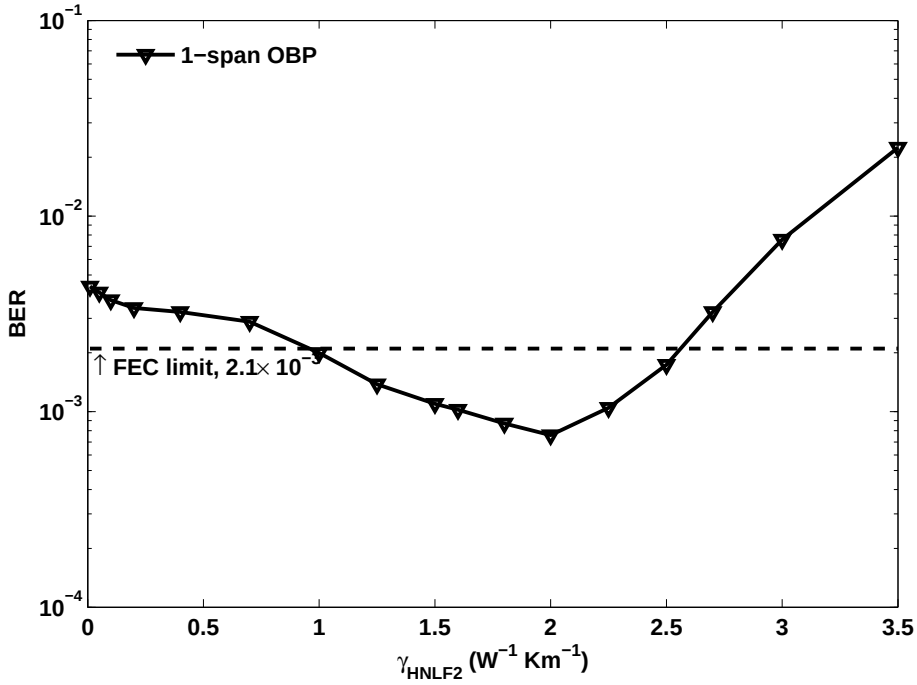

Figure 4.9: Bit error rate vs nonlinearity coefficient of HNLF2. Transmission distance = 800 Km.

Fig. 4.9 shows the BER as a function of nonlinearity coefficient of HNLF2, γ_{HNLF2}. If we carefully look at the Eq. (4.26), we will find that when

$$2\gamma_2 L_{eff,2}|u_s(t) + u_{p1}(t, L_1)|^2/3 \ll \pi. \tag{4.28}$$

The OBP and AS-DBP should lead to the same solution for the inverse NLS equation, and therefor, they should have the same performance. As it can be seen from Fig. 4.9, when product of effective length of HNLF2, $L_{eff,2}$, and nonlinear coefficient of HNLF2 ,γ_{HNLF2} is small enough these two schemes should have the same performance ($\sim 1\text{W}^{-1}\text{Km}^{-1}$), but when it is large, the linear approximation done in Eq. (4.26)

for XPM breaks down leading to performance degradations. On the other hand, if the product is too low, NLC would not compensate for transmission fiber nonlinear effects. In all of our simulations for OBP, we have optimize all of the parameters to get the best performance. Therefor, Eq. (4.28) is partially satisfied and other terms from Eq. (4.26) are contributing to the final solution which in this case leads to the better system performance.

4.3.2 Sensitivity Analysis

Eqs. (4.24) and (4.22) are only valid if the dispersion is equal to zero, but in reality it is hard to maintain zero dispersion throughout all the fiber during manufacturing process and dispersion value varies slowly in different parts of the fiber. Let us introduce the term called dispersion correlation length (DCL) which is the length that fiber segment in which dispersion can assume to have constant dispersion value and this value can be modeled as a Gaussian random variable with zero mean and the standard deviation (STD), β_{DCL}. Due to advanced fabrication techniques β_{DCL} can be smaller than 0.5 ps^2/Km.

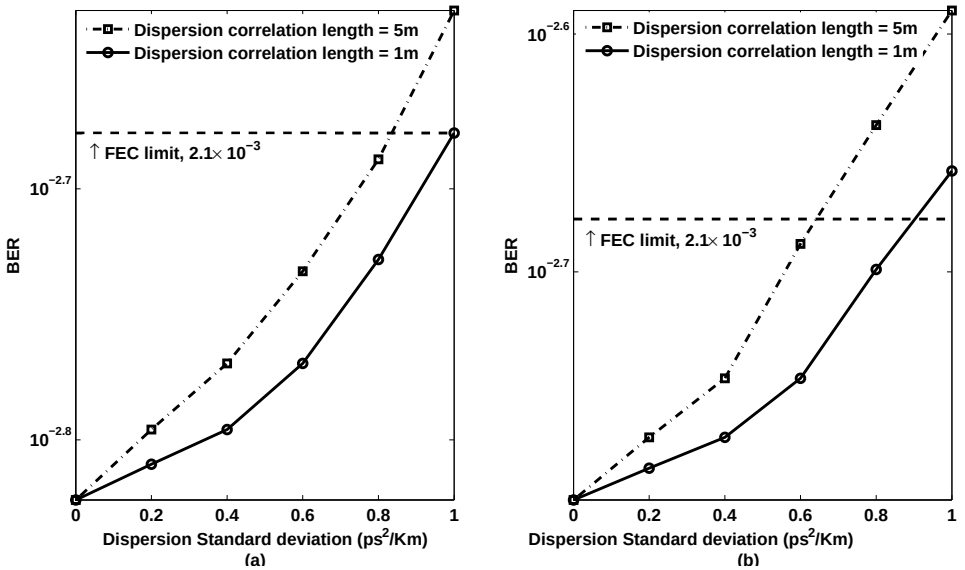

Figure 4.10: Bit error rate vs dispersion standard deviation of HNLF1 and HNLF2. (a) IONC Transmission distance = 1440 Km, (b) OBP Transmission distance = 1040 Km.

In this section, we have used the split-step Fourier method (SSFM) instead of analytical solution to simulate the system to investigate the effect of dispersion in OBP and IONC. Fig. 4.10 shows the BER as a function of dispersion standard deviation of HNLF1 and HNLF2 with dispersion correlation length equals to 1 m and 5 m for OBP and IONC. As can be seen, system performance is not affected for the STD smaller than 0.5 ps^2/Km, and therefor, these systems have reasonably good tolerance for this situation, and there is no performance degrading due to random fluctuation in fiber dispersion.

4.4 Conclusion

In conclusion, an optical back propagation and inline optical nonlinear compensation techniques can effectively undo the fiber dispersion and nonlinear effects. An optical nonlinear compensation module consists of two highly nonlinear fibers to compensate for the nonlinear phase shift accumulated over a specific fiber link length and dispersion compensating fibers to mitigate the fiber dispersion distortions. Numerical simulations show that the transmission performance can be greatly improved using optical back propagation (OBP) and inline optical nonlinear compensation (IONC). The OBP and IONC have the following advantages over DBP. (i) DBP is currently limited to compensate the nonlinear impairments of a single channel. It would be very challenging to implement DBP for wavelength division multiplexed system (WDM) in real time since the computational effort and bandwidth required in this case would be enormous. In contrast, OBP and IONC can compensate for all the channels of a WDM system simultaneously without additional cost provided the DCF and HNLFs are designed for wide band applications. (ii) OBP and IONC can be used for direct detection systems as well as for coherent detection, but DBP works only for coherent detection. (iii) OBP and IONC provide the compensation of dispersion and nonlinearity in real time whereas DBP is currently limited to off-line signal processing.

Chapter 5

Conclusions and Future Work

The rapid development of fiber optic communication systems requires higher transmission data rate and longer reach. This thesis deals with analysis of nonlinear phase noise and other limiting factors in design of long-haul fiber optic communication systems such as the fiber Ker effect and chromatic dispersion. A novel optical compensation technique to mitigate fiber impairments is also studied in this thesis.

Fiber optic communication systems use optical amplification to increase the repeater spacing and wavelength division multiplexing for increasing the bit rate. Inline optical amplifiers change the amplitude of the optical field envelope randomly and fiber nonlinear effects such as self phase modulation (SPM) convert the amplitude fluctuations to phase fluctuations which is known as nonlinear phase noise. For M-ary phase shift keying (PSK) signals, symbol error probability is determined solely by the probability density function (PDF) of the phase. Under the Gaussian PDF assumption, the phase variance can be related to the symbol error probability for PSK signals. We have also showed that the analytical formula given in this chapter for the variance of nonlinear phase noise can be used to optimize the system parameters

for dispersion-managed coherent fiber optic systems based on phase shift keying more easily without requiring extensive computational efforts for Monte-Carlo simulation.

In this thesis, we also studied an improved optical signal processing techniques such as optical backward propagation (OBP) and inline optical nonlinearity compensation (IONC), to mitigate the fiber impairments in optical communication systems. OBP and IONC use optical nonlinearity compensators (NLCs) and dispersion compensating fibers (DCFs) to compensate for the fiber nonlinearity and chromatic dispersion, respectively versos digital backward propagation (DBP) which uses the high-speed digital signal processing (DSP) unit to compensate for the fiber nonlinearity and dispersion in digital domain. NLC uses highly nonlinear fibers to impart a phase shift that is equal in magnitude to the nonlinear phase shift due to Fiber propagation, but opposite in sign. In principle, BP schemes could undo the deterministic (bit-pattern dependent) nonlinear impairments, but it can not compensate for the stochastic nonlinear impairments such as nonlinear phase noise. Our Numerical simulations show that the transmission performance can be greatly improved using OBP and IONC. Using IONC, the transmission reach becomes almost twice of DBP with the following advantage, It can compensate the nonlinear impairments for all the channels of a wavelength division multiplexed system (WDM) in real time while it would be very challenging to implement DBP for such systems due to its computational cost and bandwidth requirement. OBP and IONC can be used for direct detection systems as well as for coherent detection while they provide the compensation of dispersion and nonlinearity in real time, but DBP works only for coherent detection and currently limited to off-line signal processing.

Finally, there are still some work, that can be done in the future. In chapter 3,

only interaction between dispersion, SPM and ASE on a single pulse is considered, but in some fiber optic system set up, interaction between IXPM and ASE, could be important therefore, The interaction of SPM, IXPM and ASE for arbitrary data sequence can be investigated using perturbation theory in the future works. In optical backward propagation (OBP) simulation only 1-span and 2-span OBP schemes have been investigated but based on the theoretical result if we use smaller step size in backward propagation the system performance should increase further. Therefor, half-span OBP and quarter-span OBP can be implemented in future. The research outcomes obtained in this thesis mainly result from the computer-aided simulation. Therefore, in future, to better verify the results, more efforts will be made in the experimental investigation.

Appendix A

Linear, First-Order and Second-Order Nonlinear Solutions of NLS Equation

A.1 Gauss-Hermite Solutions (Linear Solution)

Consider the Schrodinger equation given by Eq. (3.11) with $\gamma = 0$ and $R = 0$. Using the lens-like transformation

$$u(z,t) = \sqrt{p(z)}\nu[p(z)t, z]\exp(iC(z)t^2/2) \tag{A.1}$$

in Eq. (3.11) with $\gamma = R = 0$ leads to

$$\begin{aligned} i\left(\frac{\partial \nu}{\partial z} + K_0 \tau \frac{\partial \nu}{\partial \tau}\right) &- \frac{\beta_2(z) p^2(z)}{2} \frac{\partial^2 \nu}{\partial \tau^2} \\ &= \frac{(\dot{C} - C^2 \beta_2)\tau^2}{2p^2}\nu - \frac{iK_0}{2}\nu = 0, \end{aligned} \tag{A.2}$$

where

$$K_0 = \frac{\dot{p} - C\beta_2 p}{p} \tag{A.3}$$

$\tau = p(z)t$, and . denotes the differentiation with respect to the argument. Dividing Eq. (A.2) by $\beta_2 p^2$, we get

$$i\frac{\partial \nu}{\partial \acute{z}} - \frac{1}{2}\frac{\partial^2 \nu}{\partial \tau^2} + \frac{K_1 \tau^2 \nu}{2} = 0, \tag{A.4}$$

where

$$\acute{z} = \int_0^z \beta_2(s) p^2(s) ds, \tag{A.5}$$

$$K_1 = \frac{C^2 \beta_2 - \dot{C}}{\beta_2 p^4}. \tag{A.6}$$

If we choose

$$K_1 = \frac{C^2 \beta_2 - \dot{C}}{\beta_2 p^4} = \text{constant}(= 1), \tag{A.7}$$

and

$$K_0 = \frac{p - C^2 \beta_2 p}{p} = 0 \tag{A.8}$$

we obtain

$$i\frac{\partial \nu}{\partial \acute{z}} - \frac{1}{2}\frac{\partial^2 \nu}{\partial \tau^2} + \frac{\tau^2 \nu}{2} = 0. \tag{A.9}$$

Let

$$\nu(\acute{z},\tau) = \phi_j(\tau)\exp(i\lambda_j \acute{z}), \quad j = 0,1,2,... \tag{A.10}$$

Substituting Eq. (A.10) in Eq.(A.9), we obtain

$$\frac{1}{2}\frac{d^2\phi_j}{d\tau^2} - \frac{\tau^2\phi_j}{2} = -\lambda_j\phi_j, \tag{A.11}$$

The above equation is the eigenvalue equation corresponding to the quantum harmonic oscillator. The eigenfunction ϕ_j equals Gauss-Hermite functions of Eq. (A.11) and the eigenvalue λ_j is given by

$$\lambda_j = 2j + 1. \tag{A.12}$$

The constraints imposed in Eqs. (A.7) and (A.8) on $p(z)$ and $C(z)$ with the initial condition $p(0) = l/T_0$ and $C(0) = 0$ lead to the following solution,

$$p(z) = \frac{T_0}{\sqrt{T_0^4 + S^2(z)}}, \quad C(z) = \frac{S(z)p^2(z)}{T_0^2}, \tag{A.13}$$

Note that Eq. (A.13) is same as Eq. (3.23) which is obtained using Fourier transform technique. Substituting Eq.(A.13) in Eq.(A.5), we find

$$\acute{z} = \frac{1}{2}\tan^{-1}\left[\frac{S(z)}{T_0^2}\right]. \tag{A.14}$$

Combining Eqs. (A.l),(A.l0) and (A.12), we obtain the final solution

$$u(z,t) = \sqrt{p(z)}k_j H_j(pt) exp[iC(z)t^2/2 + i(2j+1)\theta_0(z)], \tag{A.15}$$

To our knowledge, the above solution was first obtained by Lazaridis et. al. for temporal pulse propagation using a different approach.

A.2 First-Order and Second-order Nonlinear Solutions

Consider the nonlinear Schrodinger Eqs. (3.17) and (3.18)

$$i\frac{\partial u_1}{\partial z} - \frac{\beta_2}{2}\frac{\partial^2 u_1}{\partial t^2} = -a^2(z)|u_0|^2 u_0 \tag{A.16}$$

and

$$i\frac{\partial u_1}{\partial z} - \frac{\beta_2}{2}\frac{\partial^2 u_1}{\partial t^2} = -a^2(z)(2|u_0|^2 u_1 + u_0^2 u_1^*). \tag{A.17}$$

To solve these two equations, we first derive the following identity. Consider a differential equation

$$i\frac{\partial f}{\partial z} - \frac{\beta_2}{2}\frac{\partial^2 f}{\partial t^2} = F(z,t) \tag{A.18}$$

where the forcing function $F(z,t)$ is of the form

$$F(z,t) = \eta(z) \times \exp\left\{\sum_{m-1}^{2}[t - C_m(z)]^2 R_m(z) - ik(z)t\right\}. \tag{A.19}$$

Taking the Fourier transform of Eq. (A.18), we have

$$i\frac{\partial \tilde{f}(z,\omega)}{\partial z} - \frac{i\omega^2\beta_2(z)}{2}\tilde{f}(z,\omega) = i\tilde{F}(z,\omega) \tag{A.20}$$

where $\tilde{f}(z,\omega)$ is the Fourier transform of $f(z,t)$ and

$$\begin{aligned}\tilde{F}(z,\omega) &= \eta(z)\exp\left[-\sum_{m=1}^{2} C_m^2 R_m+\right]\int_{-\infty}^{+\infty}\exp\left[-Rt^2-it(C_3+2iC_r-\omega)\right]dt \\ &= \sqrt{\frac{\pi}{R}}\eta'\exp\left[\frac{-\omega^2}{4R}-\omega D\right] \qquad (A.21)\end{aligned}$$

where

$$R = R_1+R_2, \qquad (A.22)$$

$$\bar{R} = \frac{R_1R_2}{R_1+R_2}, \qquad (A.23)$$

$$C_r = C_1R_1+C_2R_2, \qquad (A.24)$$

$$D = -\frac{C_3+2iC_r}{2R} \quad \text{and} \qquad (A.25)$$

$$\eta' = \eta\exp\left[-\sum_{m=1}^{2} C_m^2R_m+\frac{4C_r^2-C_3^2-4iC_rC_3}{4R}\right]. \qquad (A.26)$$

The solution of Eq. (A.20) with initial condition $\tilde{f}(z,\omega)=0$ is

$$\tilde{f}(z,t) = -i\int_0^z \tilde{F}(z,\omega)\exp\left[\frac{i\omega^2A(z,s)}{4}\right]ds \qquad (A.27)$$

where

$$A(z) = 2[S(z)-S(s)] \qquad (A.28)$$

and

$$S(z) = \int_0^z \beta_2(x)dx. \qquad (A.29)$$

Using Eqs (A.21) and (A.26) and inverse Fourier transforming, we obtain

$$f(z,t) = \frac{-i}{2\sqrt{\pi}} \int_0^z \frac{\eta'(s)}{\sqrt{R(s)}} \times \int_{-\infty}^{+\infty} \exp\left[-\frac{\omega^2\delta}{4} - \omega(D+it)\right] d\omega ds, \tag{A.30}$$

where

$$\delta(s,z) = \frac{1}{R(s)} - iA(s,z). \tag{A.31}$$

After evaluating the inner integral in (A.29), we obtain

$$f(z,t) = -i \int_0^z \frac{\eta'(s)}{\sqrt{\delta(s,z)R(s)}} \exp\left[-\frac{(D(s)+it)^2}{\delta(s,z)}\right]. \tag{A.32}$$

Using Eqs. (A.22) to (A.25) and (A.31), the solution of Eq. (A.18) can be simplified as

$$\begin{aligned} f(z,t) = -i \int_0^z \frac{\eta(s)}{\sqrt{\delta(z,s)R(s)}} \quad &\times \quad \exp\left[-\bar{R}(C_1 - C_2)^2 + \frac{kA(k+4i\bar{C}R)}{4R\delta}\right] \\ &\times \quad \exp\left[\frac{(t-\bar{C})^2 R + ikt}{R\delta}\right] ds \end{aligned} \tag{A.33}$$

where

$$R = R_1 + R_2, \tag{A.34}$$

$$\bar{R} = \frac{R_1 R_2}{R_1 + R_2}, \tag{A.35}$$

$$\bar{C} = \frac{C_1 R_1 + C_2 R_2}{R_1 + R_2} \quad \text{and} \tag{A.36}$$

$$\delta = \frac{1}{R} - iA. \tag{A.37}$$

$$\tag{A.38}$$

To find first-order solution we make use of the the result given by Eq. (A.32) and the forcing function $F(z,t)$ in this case is

$$F(z,t) = a^2(z)\,|u_0|^2\,u_0, \tag{A.39}$$

where u_0 is given by Eq. (3.21). Therefore, the firs order solution u_1 is given by

$$u_1(z,t) = \gamma|E|\sqrt{E}g^{(1)}(z,t)F(z,t), \tag{A.40}$$

where

$$g^{(1)}(z,t) = j\frac{T_0^2}{\sqrt{\pi}}\int_0^z \frac{\exp(-a(s)-\Delta(s)t^2)}{T_1(s)|T_1^2(s)|\sqrt{\delta(z,s)R(s)}}ds \tag{A.41}$$

and

$$\begin{aligned}
a(s) &= \exp(-\alpha s/2), && \text{(A.42)}\\
T_1^2(s) &= T_0^2 - iS(s), && \text{(A.43)}\\
T_2^2(s) &= \frac{|T_0^2 - iS(s)|^2}{2T_0}, && \text{(A.44)}\\
R(s) &= \frac{T_1^2(s)+T_2^2(s)}{2T_1^2(s)T_2^2(s)}, && \text{(A.45)}\\
\delta(s,z) &= \frac{1}{R(s)} - iA(s,z), && \text{(A.46)}\\
\Delta(s,z) &= \frac{1}{\delta_y(s,z)} - \frac{1}{2T_0^2} \quad \text{and} && \text{(A.47)}\\
A(s,z) &= 2[S(z)-S(s)]. && \text{(A.48)}
\end{aligned}$$

Similarly, the second-order solution can be found by repeating the same procedure and the forcing function $F(z,t)$ in this case is

$$F(z,t) = -a^2(z)\left(2\left|u_0\right|^2 u_1 + u_0^2 u_1^*\right) \tag{A.49}$$

where u_0 and u_1 are given by Eqs. (3.21) and (3.27), respectively. Therefore, the second-order solution u_2 is calculated as

$$u_2(z,t) = \gamma^2|E|^2\sqrt{E}g^{(2)}(z,t)F(z,t), \tag{A.50}$$

and $g^{(2)}(z,t)$ can be found as

$$g^{(2)}(z,t) = -2g_x^{(2)}(z,t) + g_y^{(2)}(z,t) \tag{A.51}$$

here

$$g_x^{(2)}(z,t) = \frac{T_0^3}{\pi}\int_0^z\int_0^s \frac{\exp(-a(s+s') - \Delta_x(s)t^2)}{T_1(s')|T_1^2(s')||T_1^2(s)|\sqrt{\delta(s,s')R(s')}} \times \frac{dsds'}{\sqrt{\delta_x(s,s',z)R_x(s,s')}} \tag{A.52}$$

and

$$g_y^{(2)}(z,t) = \frac{T_0^3}{\pi}\int_0^z\int_0^s \frac{\exp(-a(s+s') - \Delta_x(s)t^2)}{T_1^*(s')|T_1^2(s')|T_1^2(s)\sqrt{\delta^*(s,s')R^*(s')}} \times \frac{dsds'}{\sqrt{\delta_y(s,s',z)R_y(s,s')}} \tag{A.53}$$

where

$$R_x(s,s') = \frac{1}{T_1^2(s)} + \frac{1}{\delta(s,s')}, \tag{A.54}$$

$$\delta_x(s,s',z) = \frac{1}{R_x(s,s')} - iA(s,z), \tag{A.55}$$

$$\Delta_x(s,s',z) = \frac{1}{\delta_x(s,s',z)} - \frac{1}{2T_0^2}, \tag{A.56}$$

$$R_y(s,s') = \frac{1}{T_1^2(s)} + \frac{1}{\delta^*(s,s')}, \tag{A.57}$$

$$\delta_y(s,s',z) = \frac{1}{R_y(s,s')} - iA(s,z) \quad \text{and} \tag{A.58}$$

$$\Delta_y(s,s',z) = \frac{1}{\delta_y(s,s',z)} - \frac{1}{2T_0^2}. \tag{A.59}$$

Bibliography

[1] M. Abrams, P.C. Becker, Y. Fujimoto, V. O'Byrne, and D. Piehler. Fttp deployments in the united states and japan-equipment choices and service provider imperatives. *Lightwave Technology, Journal of*, 23(1):236–246, 2005.

[2] T.H. Maiman. Stimulated optical radiation in ruby. 1960.

[3] FP Kapron, DB Keck, and RD Maurer. Radiation losses in glass optical waveguides. *Applied Physics Letters*, 17(10):423–425, 1970.

[4] T. Miya, Y. Terunuma, T. Hosaka, and T. Miyashita. Ultimate low-loss single-mode fibre at 1.55 um. *Electronics Letters*, 15(4):106–108, 1979.

[5] G.P. Agrawal. *Fiber-optic communication systems*. Wiley New York, 1997.

[6] LG Cohen, C. Lin, and WG French. Tailoring zero chromatic dispersion into the 1.5–1.6 μm low-loss spectral region of single-mode fibres. *Electronics Letters*, 15:334, 1979.

[7] KC Byron. Simultaneous amplification and pulse compression in a single-mode optical fibre. *Electronics Letters*, 22(24):1275–1277, 1986.

[8] H.J. Shaw and M.J.F. Digonnet. Fiber optic amplifier, June 23 1987. US Patent 4,674,830.

[9] G.P. Agrawal. *Nonlinear fiber optics*. Academic Press, 2001.

[10] W. Shieh and I. Djordjevic. *OFDM for optical communications*. Academic Press, 2009.

[11] I. Shake, H. Takara, K. Mori, S. Kawanishi, and Y. Yamabayashi. Influence of inter-bit four-wave mixing in optical tdm transmission. *Electronics Letters*, 34(16):1600–1601, 1998.

[12] R.J. Essiambre, B. Mikkelsen, and G. Raybon. Intra-channel cross-phase modulation and four-wave mixing in high-speed tdm systems. *Electronics Letters*, 35(18):1576–1578, 1999.

[13] PV Mamyshev and NA Mamysheva. Pulse-overlapped dispersion-managed data transmission and intrachannel four-wave mixing. *Optics letters*, 24(21):1454–1456, 1999.

[14] E.M. Ip and J.M. Kahn. Fiber impairment compensation using coherent detection and digital signal processing. *Lightwave Technology, Journal of*, 28(4):502–519, 2010.

[15] E. Ip, A.P.T. Lau, D.J.F. Barros, and J.M. Kahn. Coherent detection in optical fiber systems. *Optics Express*, 16(2):753–791, 2008.

[16] K. Kikuchi. History of coherent optical communication and challenges for the future. In *IEEE/LEOS Summer Topical Meetings, 2008 Digest of the*, pages 107–108. IEEE.

[17] R.A. Linke and A.H. Gnauck. High-capacity coherent lightwave systems. *Lightwave Technology, Journal of*, 6(11):1750–1769, 1988.

[18] T. Okoshi and K. Kikuchi. *Coherent optical fiber communications*. Springer, 1988.

[19] S.J. Savory, G. Gavioli, R.I. Killey, and P. Bayvel. Electronic compensation of chromatic dispersion using a digital coherent receiver. *Optics Express*, 15(5):2120–2126, 2007.

[20] W. Shieh, H. Bao, and Y. Tang. Coherent optical ofdm: theory and design. *Optics Express*, 16(2):841–859, 2008.

[21] J.H. Winters and R.D. Gitlin. Electrical signal processing techniques in long-haul fiber-optic systems. *Communications, IEEE Transactions on*, 38(9):1439–1453, 1990.

[22] P.J. Winzer and R.J. Essiambre. Advanced modulation formats for high-capacity optical transport networks. *Journal of Lightwave Technology*, 24(12):4711–4728, 2006.

[23] J.G. Proakis. *Digital Communications*. McGraw-Hill, Boston, 2001.

[24] S. Tsukamoto, D.S. Ly-Gagnon, K. Katoh, K. Kikuchi, et al. Coherent demodulation of 40-gbit/s polarization-multiplexed qpsk signals with 16-ghz spacing after 200-km transmission. In *Proc. OFC*, volume 2005, page 29, 2005.

[25] E. Mateo, L. Zhu, and G. Li. Impact of xpm and fwm on the digital implementation of impairment compensation for wdm transmission using backward propagation. *Opt. Exp*, 16(20):16124–16137, 2008.

[26] J.P. Gordon and L.F. Mollenauer. Phase noise in photonic communications systems using linear amplifiers. *Optics letters*, 15(23):1351–1353, 1990.

[27] S. Ryu. Signal linewidth broadening due to fibre nonlinearities in long-haul coherent optical fibre communication systems. *Electronics Letters*, 27(17):1527–1529, 1991.

[28] S. Ryu. Signal linewidth broadening due to nonlinear kerr effect in long-haul coherent systems using cascaded optical amplifiers. *Lightwave Technology, Journal of*, 10(10):1450–1457, 1992.

[29] S. Saito, M. Aiki, and T. Ito. System performance of coherent transmission over cascaded in-line fiber amplifiers. *Lightwave Technology, Journal of*, 11(2):331–342, 1993.

[30] R.J. Essiambre, G. Raybon, and B. Mikkelsen. Pseudo-linear transmission of high-speed tdm signals: 40 and 160 gb/s. *Optical Fiber Telecommunications IVB*, pages 233–304, 2002.

[31] S. Kumar and A. Hasegawa. Quasi-soliton propagation in dispersion-managed optical fibers. *Optics letters*, 22(6):372–374, 1997.

[32] S. Kumar and D. Yang. Second-order theory for self-phase modulation and cross-phase modulation in optical fibers. *Lightwave Technology, Journal of*, 23(6):2073–2080, 2005.

[33] S. Kumar. Analysis of nonlinear phase noise in coherent fiber-optic systems based on phase shift keying. *Lightwave Technology, Journal of*, 27(21):4722–4733, 2009.

[34] M. Malekiha and S. Kumar. Second-order theory for nonlinear phase noise in coherent fiber-optic systems based on phase shift keying. pages 466–469, 2011.

[35] K.P. Ho. *Phase-modulated optical communication systems*. Springer Verlag, 2005.

[36] A.G. Green, P. Mitra, and L. Wegener. Effect of chromatic dispersion on nonlinear phase noise. *Optics letters*, 28(24):2455–2457, 2003.

[37] S. Kumar. Effect of dispersion on nonlinear phase noise in optical transmission systems. *Optics letters*, 30(24):3278, 2005.

[38] X. Li, X. Chen, G. Goldfarb, E. Mateo, I. Kim, F. Yaman, and G. Li. Electronic post-compensation of wdm transmission impairments using coherent detection and digital signal processing. *Opt. Express*, 16(2):880–888, 2008.

[39] S. Watanabe and M. Shirasaki. Exact compensation for both chromatic dispersion and kerr effect in a transmission fiber using optical phase conjugation. *Lightwave Technology, Journal of*, 14(3):243–248, 1996.

[40] E. Ip and J.M. Kahn. Compensation of dispersion and nonlinear impairments using digital backpropagation. *Journal of Lightwave Technology*, 26(20):3416–3425, 2008.

[41] E. Ip and J.M. Kahn. Nonlinear impairment compensation using backpropagation. *Optical Fibre, New Developments*.

[42] S. Kumar and D. Yang. Optical backpropagation for fiber-optic communications using highly nonlinear fibers. *Optics Letters*, 36(7):1038–1040, 2011.